ff14SB: Improving the accuracy of protein side chain and backbone parameters from ff99SB: Supporting Information

James Maier,[†,¶] Carmenza Martinez,[‡,¶] Koushik Kasavajhala,[‡,¶] Lauren Wickstrom,[†] Kevin Hauser,[‡,¶] and Carlos Simmerling[*,‡,†,¶]

Graduate Program in Biochemistry and Structural Biology, Stony Brook University, Stony Brook, NY 11794, United States of America, and Department of Chemistry, Stony Brook University, Stony Brook, NY 11794, United States of America

E-mail: carlos.simmerling@stonybrook.edu

Phone: +1 (631) 632-1336. Fax: +1 (631) 632-5405

This supplement contains additional information concerning generation of the backbone and side chain modifications. The supplement also contains the details of building HBSP and testing results for HBSP and K19. Then, representative structures from cluster analysis and NOE violations, divided into backbone-backbone, backbone-side chain, and side chain-side chain restraints, are reported for CLN025. Analyses of side chain scalar coupling convergence and backbone dependence are presented. Then, testing of the AMBER12-bundled ff12SB is compared with ff14SB presented in the main text. Finally, a table of the ff14SB parameters is included.

[*]To whom correspondence should be addressed

[†]Graduate Program in Biochemistry and Structural Biology, Stony Brook University, Stony Brook, NY 11794, United States of America

[‡]Department of Chemistry, Stony Brook University, Stony Brook, NY 11794, United States of America

[¶]Laufer Center for Physical and Quantitative Biology, Stony Brook University, Stony Brook, NY 11794, United States of America

Additional training information

Sparse grids for long side chains

For amino acids with long side chains for which a comprehensive grid-based approach was intractable, broad distributions of structures were still desirable. We therefore used simulations maintained at 500 K by a Langevin thermostat to efficiently explore the moderately accessible conformation space of lysine, arginine, glutamate, glutamic acid, glutamine, and methionine dipeptides for 100 ns. Restraints of 2×10^3 kcal/mol/rad on ϕ and ψ maintained the backbone throughout. In a vacuum, the side chains would predominantly sample one or two conformations stabilized by electrostatic interactions with the backbone. To avoid such electrostatic traps, a $4r$ dielectric was applied. The simulations were integrated with a 1 fs timestep. Structures were saved every 2 fs to capture short-lived transitions.

The resulting structures were then mapped onto multi-dimensional grids across all side chain dihedrals, for each amino acid at each of α and β backbone conformations, spaced 10° in each side chain dihedral. To ensure a relatively even distribution of conformations, only the five lowest potential energy structures were saved at each grid point. In this way, only extremely sparse conformations (with 4 or less frames each representing 2 fs of a 100 ns simulation) were less represented. Five hundred of these saved structures were then randomly extracted from each grid.

To generate sets of structures that varied principally in side chain conformation, minor differences in backbone conformation had to be reconciled. For each set of structures, the average value of every backbone dihedral was determined. Each structure was minimized for 100 000 cycles using ff99SB, with incremental restraints on the dihedrals describing all four-atom torsions within the backbone to their average values at weights of 100 kcal/mol/rad^2, 500 kcal/mol/rad^2, 1×10^3 kcal/mol/rad^2, 5×10^3 kcal/mol/rad^2, and then 1×10^4 kcal/mol/rad^2, for 500 cycles each, and finally 1.5×10^4 kcal/mol/rad^2 for the remainder of minimization. Side chain restraints were included as described in the main

text. The methyl groups at the N- and C-termini, due to their C3 symmetry, were not restrained to their average values but to $-5°$ for one of the H−C−C−N and 60° for one of the C−N−C−H dihedrals.The simulations generated some structures with challenging sterics or electrostatics, where atoms were within close proximity. One concern is that the molecular mechanical model employs charges that are fixed for a dielectric. A second concern is that the r^{-12} Lennard-Jones approximation of repulsion is an unphysical mathematical convenience (the dispersive r^{-6} squared) that may be too hard at close range. We did not want to fit the errors of fixed charges in a vacuum, nor possible MM repulsion artifacts. Thus, structures where the distances between atoms not in a bond or angle breached the sum of their van der Waals radii[1] divided by 1.3 were eliminated. The scaling factor 1.3 was chosen empirically as a value that left a reasonable number of structures in the training set but targeted those with the greatest degree of contact.

A second non-bonded filter specifically targeted strong electrostatic interactions. When the Coulombic energy between a side chain particle pair exceeded 42 kcal/mol in magnitude, the interaction was evaluated "very strong" and the structure was discarded from the training set. As with the inter-atomic scaling factor, 42 was chosen for its qualitative ability to remove the most extreme of electrostatic interactions. Any number between 40 and 43 kcal/mol selected conformations with the greatest degree of side chain-backbone electrostatic interactions, but 42 received preference based on previous work.[2] For this Coulombic energy evaluation, the Cornell et al.[3,4] RESP charge set and MP2/6-31+G** Mulliken charges were considered.

Structures with energies more than 30 kcal/mol greater than the minimum energy for that combination of amino acid and backbone conformation were considered overly strained and were also therefore removed from the training. The final number of conformations for each amino acid is tabulated in Table S4 on page 14.

Quantum calculations for the above residues were carried out using Gaussian 98[5] using default options.

Fitting details

Six populations of 63 individuals each were created: two with ff99SB parameters, two with zero parameters, and two with random parameters created with different random seeds. Each set of populations was then subjected to a series of evolutions using random seeds 314 159 and 271 828, carried out using GAlib.[6] An elitist regime maintained the fittest tenth of the population from one generation to the next. Initially, each population evolved for 200 000 generations at a mutation rate of 0.01 and crossover rate of 0.8. Mutation rate defined the probability with which a given parameter pair—amplitude and phase shift—will mutate. Upon mutation, the random value was used to determine whether the amplitude or the phase shift will change. Perturbation to amplitude, *mutateBy*, depended upon mutation rate and the random number, by the relation in Equation (1), where *random* is a random number between 0 and 1, and *mutRate* is the mutation rate:

$$mutateBy = \begin{cases} random/mutRate - 0.5, & random < mutRate \\ 0, & random \geq mutRate \end{cases} \tag{1}$$

This scheme alternated with a second, where all changes to amplitude were 0.001 kcal/mol in magnitude. If perturbing the phase shift, the lowest bit of the random number determined whether the phase shift would be 0 or 180 degrees.

To narrowly locate sets of parameters that minimize error after the first 200 000 generations, each population was continued with a mutation rate of 0.005 and crossover rate of 0.8 with the second scheme, then 0.002 and 0.8 with the first and second scheme, and finally 0.001 and 0.8 with the first and second scheme until convergence.

Convergence was evaluated as a run starting from ff99SB finding the same steady (less than 0.001 improvement in 10 000 generations) solution as a run starting from zero or random parameters. Solutions were considered the same if the correction energy profile scanned every 10° was identical within 0.01 kcal/mol.

Fitting χ1 N-Cα-Xβ-Xγ and C-Cα-Xβ-Xγ parameters required consideration of the sp3 hybridization of the α-carbon. Multiple three-fold dihedral corrections cannot be partitioned between the N and the C, as they are rotated 120° relative to the Cα-Xβ bond; the same three-fold correction must be applied to both. In the AMBER12-bundled ff12SB, we did not account for this, and so amplitudes like the three-fold around χ1 were of arbitrary magnitude, with potentially undesirable effects on small peptides like Val_3 and loop regions. Other periodicity terms, however, were trained separately, such as one-fold corrections around χ1 describing whether the side chain γ substituent should be placed gauche to the N, the C, or both.

Where amino acids had planar moieties, however, there were multiple sets of 4-atom combinations with dihedrals offset by 180°. In these cases, it was necessary to choose a single set of atom types to apply corrections to, as a 180° offset means odd-periodicity terms will be out-of-phase, and have exactly opposite effects, while even-periodicity terms will be in-phase, and thus cannot be distinguished. In the case of amide and carboxylic groups sharing atom types, we only fit the terms correcting C-C-C-OH and C-C-C-N, as these are distinct between the two.

In the case of histidine, the various atom types of the different protonation states required us to fit multiple corrections. Histidine has two χ2 non-hydrogen dihedrals, to the Nδ and to the Cδ. Histidine Nδ1 and Cδ2 are atom types NA and CV in δ-protonated histidine, NB and CW in ϵ-protonated histidine, and NA and CW in ionic histidine. Since only δ-protonated histidine possessed a χ2 CV and only ϵ-protonated histidine possessed a χ2 NB, it seemed logical to fit one of these χ2 corrections independently, while fitting the remaining two protonation states with two sets of corrections. We tried both and chose fitting Hie separately as the combination that best fit the quantum data.

Table S1: The amino acids and the bonds that have been corrected, the four atom combinations, and the atom types of each correction that has been modified. This table has the same contents as Table S2 on page 10, but sorted by amino acid.

Amino acid	Rotatable bond	Atom names	Atom types	Solving group
Arg	$\chi 1$	N-C_α-C_β-C_γ*	N-CX-C8-C8	6
		C-C_α-C_β-C_γ	C-CX-C8-C8	
	$\chi 2$	C_α-C_β-C_γ-C_δ*	CX-C8-C8-C8	
	$\chi 3$	C_β-C_γ-C_δ-N_ϵ*	C8-C8-C8-N2	
	$\chi 4$	C_γ-C_δ-N_ϵ-C_ζ*	C8-C8-N2-CA	
Ash	$\chi 1$	N-C_α-C_β-C_γ*	N-CX-2C-C	3
		C-C_α-C_β-C_γ	C-CX-2C-C	
	$\chi 2$	C_α-C_β-C_γ-$O_{\delta 1}$*	CX-2C-C-O	
		C_α-C_β-C_γ-$O_{\delta 2}$	CX-2C-C-OH	
	oh	C_β-C_γ-$O_{\delta 2}$-$H_{\delta 2}$*	2C-C-OH-HO	
Asn	$\chi 1$	N-C_α-C_β-C_γ*	N-CX-2C-C	3
		C-C_α-C_β-C_γ	C-CX-2C-C	
	$\chi 2$	C_α-C_β-C_γ-$O_{\delta 1}$*	CX-2C-C-O	
		C_α-C_β-C_γ-$N_{\delta 2}$	CX-2C-C-N	
Asp	$\chi 1$	N-C_α-C_β-C_γ*	N-CX-2C-CO	9
		C-C_α-C_β-C_γ	C-CX-2C-CO	
	$\chi 2$	C_α-C_β-C_γ-$O_{\delta 1}$*	CX-CS-CO-O2	
		C_α-C_β-C_γ-$O_{\delta 2}$	CX-CS-CO-O2	
Cys	$\chi 1$	N-C_α-C_β-S_γ*	N-CX-2C-SH	7
		C-C_α-C_β-S_γ	C-CX-2C-SH	
	$\chi 2$	C_α-C_β-S_γ-H_γ*	CX-2C-SH-HS	
Cyx	$\chi 1$	N-C_α-C_β-S_γ*	N-CX-2C-S	0
		C-C_α-C_β-S_γ	C-CX-2C-S	

Amino acid	Rotatable bond	Atom names	Atom types	Solving group
	$\chi 2$	C_α-C_β-S_γ-$S_{\gamma'}$*	CX-2C-S-S	
	χ_{SS}	C_β-S_γ-$S_{\gamma'}$-$C_{\beta'}$*	2C-S-S-2C	
Glh	$\chi 1$	N-C_α-C_β-C_γ*	N-CX-2C-2C	1
		C-C_α-C_β-C_γ	C-CX-2C-2C	
	$\chi 2$	C_α-C_β-C_γ-C_δ*	CX-2C-2C-C	
	$\chi 3$	C_β-C_γ-C_δ-$O_{\epsilon 1}$*	2C-2C-C-OH	
		C_β-C_γ-C_δ-$O_{\epsilon 2}$	2C-2C-C-OH	
Gln	$\chi 1$	N-C_α-C_β-C_γ*	N-CX-2C-2C	1
		C-C_α-C_β-C_γ	C-CX-2C-2C	
	$\chi 2$	C_α-C_β-C_γ-C_δ*	CX-2C-2C-C	
	$\chi 3$	C_β-C_γ-C_δ-$O_{\epsilon 1}$*	2C-2C-C-O	
		C_β-C_γ-C_δ-$N_{\epsilon 2}$	2C-2C-C-N	
Glu	$\chi 1$	N-C_α-C_β-C_γ*	N-CX-2C-2C	1
		C-C_α-C_β-C_γ	C-CX-2C-2C	
	$\chi 2$	C_α-C_β-C_γ-C_δ*	CX-2C-2C-CO	
	$\chi 3$	C_β-C_γ-C_δ-$O_{\epsilon 1}$*	2C-2C-C-O2	
		C_β-C_γ-C_δ-$O_{\epsilon 2}$	2C-2C-C-O2	
Hid	$\chi 1$	N-C_α-C_β-C_γ*	N-CX-CT-CC	4
		C-C_α-C_β-C_γ	C-CX-CT-CC	
	$\chi 2$	C_α-C_β-C_γ-$N_{\delta 1}$*	CX-CT-CC-NA	
		C_α-C_β-C_γ-$C_{\delta 2}$	CX-CT-CC-CV	
Hie	$\chi 1$	N-C_α-C_β-C_γ*	N-CX-CT-CC	4
		C-C_α-C_β-C_γ	C-CX-CT-CC	
	$\chi 2$	C_α-C_β-C_γ-$N_{\delta 1}$*	CX-CT-CC-NB	
		C_α-C_β-C_γ-$C_{\delta 2}$	CX-CT-CC-CW	
Hip	$\chi 1$	N-C_α-C_β-C_γ*	N-CX-CT-CC	4

Amino acid	Rotatable bond	Atom names	Atom types	Solving group
		C-C_α-C_β-C_γ	C-CX-CT-CC	
	$\chi2$	C_α-C_β-C_γ-$N_{\delta1}$*	CX-CT-CC-NA	
		C_α-C_β-C_γ-$C_{\delta2}$	CX-CT-CC-CW	
Ile	$\chi1$	N-C_α-C_β-$C_{\gamma1}$*	N-CX-3C-2C	
		C-C_α-C_β-$C_{\gamma1}$	C-CX-3C-2C	
		N-C_α-C_β-$C_{\gamma2}$	N-CX-3C-CT	2
		C-C_α-C_β-$C_{\gamma2}$	C-CX-3C-CT	
	$\chi2$	C_α-C_β-$C_{\gamma1}$-$C_{\delta1}$*	CX-3C-2C-CT	
		$C_{\gamma2}$-C_β-$C_{\gamma1}$-$C_{\delta1}$	CT-3C-2C-CT	
Leu	$\chi1$	N-C_α-C_β-C_γ*	N-CX-2C-3C	10
		C-C_α-C_β-C_γ	C-CX-2C-3C	
	$\chi2$	C_α-C_β-C_γ-$C_{\delta1}$*	CX-CS-3C-CT	
		C_α-C_β-C_γ-$C_{\delta2}$	CX-CS-3C-CT	
Lys	$\chi1$	N-C_α-C_β-C_γ*	N-CX-C8-C8	6
		C-C_α-C_β-C_γ	C-CX-C8-C8	
	$\chi2$	C_α-C_β-C_γ-C_δ*	CX-C8-C8-C8	
	$\chi3$	C_β-C_γ-C_δ-C_ϵ*	C8-C8-C8-C8	
	$\chi4$	C_γ-C_δ-C_ϵ-N_ζ*	C8-C8-C8-N3	
Met	$\chi1$	N-C_α-C_β-C_γ*	N-CX-2C-2C	1
		C-C_α-C_β-C_γ	C-CX-2C-2C	
	$\chi2$	C_α-C_β-C_γ-S_δ*	CX-2C-2C-S	
	$\chi3$	C_β-C_γ-S_δ-C_ϵ*	2C-2C-S-CT	
Phe	$\chi1$	N-C_α-C_β-C_γ*	N-CX-2C-CA	5
		C-C_α-C_β-C_γ	C-CX-2C-CA	
	$\chi2$	C_α-C_β-C_γ-$C_{\delta1}$*	CX-2C-CA-CA	

Amino acid	Rotatable bond	Atom names	Atom types	Solving group
		C_α-C_β-C_γ-$C_{\delta2}$	CX-2C-CA-CA	
Ser	$\chi1$	N-C_α-C_β-O_γ*	N-CX-2C-OH	11
		C-C_α-C_β-O_γ	C-CX-2C-OH	
	oh	C_α-C_β-O_γ-H_γ*	CX-2C-OH-HO	
Thr	$\chi1$	N-C_α-C_β-$O_{\gamma1}$*	N-CX-3C-OH	
		C-C_α-C_β-$O_{\gamma1}$	C-CX-3C-OH	
		N-C_α-C_β-$C_{\gamma2}$	N-CX-3C-CT	2
		C-C_α-C_β-$C_{\gamma2}$	C-CX-3C-CT	
	oh	C_α-C_β-$O_{\gamma1}$-$H_{\gamma1}$*	CX-3C-OH-HO	
		$C_{\gamma2}$-C_β-$O_{\gamma1}$-$H_{\gamma1}$	CT-3C-OH-HO	
Trp	$\chi1$	N-C_α-C_β-C_γ*	N-CX-CT-C*	8
		C-C_α-C_β-C_γ	C-CX-CT-C*	
	$\chi2$	C_α-C_β-C_γ-$C_{\delta1}$*	CX-CT-C*-CW	
		C_α-C_β-C_γ-$C_{\delta2}$	CX-CT-C*-CB	
Tyr	$\chi1$	N-C_α-C_β-C_γ*	N-CX-2C-CA	5
		C-C_α-C_β-C_γ	C-CX-2C-CA	
	$\chi2$	C_α-C_β-C_γ-$C_{\delta1}$*	CX-2C-CA-CA	
		C_α-C_β-C_γ-$C_{\delta2}$	CX-2C-CA-CA	
	oh	$C_{\epsilon1}$-C_ζ-O_η-H_η*	CA-C-OH-HO	
		$C_{\epsilon2}$-C_ζ-O_η-H_η	CA-C-OH-HO	
Val	$\chi1$	N-C_α-C_β-$C_{\gamma1}$*	N-CX-3C-CT	2
		N-C_α-C_β-$C_{\gamma2}$	N-CX-3C-CT	
		C-C_α-C_β-$C_{\gamma1}$	C-CX-3C-CT	
		C-C_α-C_β-$C_{\gamma2}$	C-CX-3C-CT	

Table S2: The atom types of each correction modified, the residues, bonds, and 4-atom name combinations affected

Dihedral atom types	Rotamers affected	Dihedral atom names
N-CX-C8-C8	Arg χ1	N-C_α-C_β-C_γ
	Lys χ1	
C-CX-C8-C8	Arg χ1	C-C_α-C_β-C_γ
	Lys χ1	
CX-C8-C8-C8	Arg χ2	C_α-C_β-C_γ-C_δ
	Lys χ2	
C8-C8-C8-C8	Lys χ3	C_β-C_γ-C_δ-C_ϵ
C8-C8-C8-N3	Lys χ4	C_γ-C_δ-C_ϵ-N_ζ
C8-C8-C8-N2	Arg χ3	C_β-C_γ-C_δ-N_ϵ
C8-C8-N2-CA	Arg χ4	C_γ-C_δ-N_ϵ-C_ζ
N-CX-2C-SH	Cys χ1	N-C_α-C_β-S_γ
C-CX-2C-SH	Cys χ1	C-C_α-C_β-S_γ
CX-2C-SH-HS	Cys χ2	C_α-C_β-S_γ-H_γ
N-CX-2C-S	Cyx χ1	N-C_α-C_β-S_γ
C-CX-2C-S	Cyx χ1	C-C_α-C_β-S_γ
CX-2C-S-S	Cyx χ2	C_α-C_β-S_γ-$S_{\gamma'}$
2C-S-S-2C	Cyx χ_{SS}	C_β-S_γ-$S_{\gamma'}$-$C_{\beta'}$
N-CX-CT-C*	Trp χ1	N-C_α-C_β-C_γ
C-CX-CT-C*	Trp χ1	C-C_α-C_β-C_γ
CX-CT-C*-CW	Trp χ2	C_α-C_β-C_γ-$C_{\delta1}$
CX-CT-C*-CB	Trp χ2	C_α-C_β-C_γ-$C_{\delta2}$
N-CX-2C-CO	Asp χ1	N-C_α-C_β-C_γ
C-CX-2C-CO	Asp χ1	C-C_α-C_β-C_γ
CX-CS-CO-O2	Asp χ2	C_α-C_β-C_γ-$O_{\delta1}$

Dihedral atom types	Rotamers affected	Dihedral atom names
		C_α-C_β-C_γ-$O_{\delta 2}$
N-CX-2C-C	Ash $\chi 1$	N-C_α-C_β-C_γ
	Asn $\chi 1$	
C-CX-2C-C	Ash $\chi 1$	C-C_α-C_β-C_γ
	Asn $\chi 1$	
CX-2C-C-O	Ash $\chi 2$	C_α-C_β-C_γ-$O_{\delta 1}$
	Asn $\chi 2$	
CX-2C-C-OH	Ash $\chi 2$	C_α-C_β-C_γ-$O_{\delta 2}$
CX-2C-C-N	Asn $\chi 2$	C_α-C_β-C_γ-$N_{\delta 2}$
N-CX-2C-OH	Ser $\chi 1$	N-C_α-C_β-O_γ
C-CX-2C-OH	Ser $\chi 1$	C-C_α-C_β-O_γ
CX-2C-OH-HO	Ser oh	C_α-C_β-O_γ-H_γ
N-CX-2C-3C	Leu $\chi 1$	N-C_α-C_β-C_γ
C-CX-2C-3C	Leu $\chi 1$	C-C_α-C_β-C_γ
CX-CS-3C-CT	Leu $\chi 2$	C_α-C_β-C_γ-$C_{\delta 1}$
		C_α-C_β-C_γ-$C_{\delta 2}$
N-CX-3C-CT	Ile $\chi 1$	N-C_α-C_β-$C_{\gamma 2}$
	Thr $\chi 1$	
	Val $\chi 1$	N-C_α-C_β-$C_{\gamma 1}$
		N-C_α-C_β-$C_{\gamma 2}$
C-CX-3C-CT	Ile $\chi 1$	C-C_α-C_β-$C_{\gamma 2}$
	Thr $\chi 1$	
	Val $\chi 1$	C-C_α-C_β-$C_{\gamma 1}$
		C-C_α-C_β-$C_{\gamma 2}$
N-CX-3C-2C	Ile $\chi 1$	N-C_α-C_β-$C_{\gamma 1}$

Dihedral atom types	Rotamers affected	Dihedral atom names
C-CX-3C-2C	Ile $\chi 1$	C-C_α-C_β-$C_{\gamma 1}$
N-CX-3C-OH	Thr $\chi 1$	N-C_α-C_β-$O_{\gamma 1}$
C-CX-3C-OH	Thr $\chi 1$	C-C_α-C_β-$O_{\gamma 1}$
CX-3C-2C-CT	Ile $\chi 2$	C_α-C_β-$C_{\gamma 1}$-$C_{\delta 1}$
CT-3C-2C-CT	Ile $\chi 2$	$C_{\gamma 2}$-C_β-$C_{\gamma 1}$-$C_{\delta 1}$
CX-3C-OH-HO	Thr oh	C_α-C_β-$O_{\gamma 1}$-$H_{\gamma 1}$
N-CX-2C-CA	Phe $\chi 1$	N-C_α-C_β-C_γ
	Tyr $\chi 1$	
C-CX-2C-CA	Phe $\chi 1$	C-C_α-C_β-C_γ
	Tyr $\chi 1$	
CX-2C-CA-CA	Phe $\chi 2$	C_α-C_β-C_γ-$C_{\delta 1}$
	Tyr $\chi 2$	C_α-C_β-C_γ-$C_{\delta 2}$
CA-C-OH-HO	Tyr oh	$C_{\epsilon 1}$-C_ζ-O_η-H_η
		$C_{\epsilon 2}$-C_ζ-O_η-H_η
N-CX-CT-CC	Hid $\chi 1$	N-C_α-C_β-C_γ
	Hie $\chi 1$	
	Hip $\chi 1$	
C-CX-CT-CC	Hid $\chi 1$	C-C_α-C_β-C_γ
	Hie $\chi 1$	
	Hip $\chi 1$	
CX-CT-CC-NA	Hid $\chi 2$	C_α-C_β-C_γ-$N_{\delta 1}$
	Hip $\chi 2$	
CX-CT-CC-NB	Hie $\chi 2$	C_α-C_β-C_γ-$N_{\delta 1}$
CX-CT-CC-CV	Hid $\chi 2$	C_α-C_β-C_γ-$C_{\delta 2}$
CX-CT-CC-CW	Hie $\chi 2$	C_α-C_β-C_γ-$C_{\delta 2}$

Dihedral atom types	Rotamers affected	Dihedral atom names
	Hip $\chi 2$	
N-CX-2C-2C	Glh $\chi 1$	N-C_α-C_β-C_γ
	Gln $\chi 1$	
	Glu $\chi 1$	
	Met $\chi 1$	
C-CX-2C-2C	Glh $\chi 1$	C-C_α-C_β-C_γ
	Gln $\chi 1$	
	Glu $\chi 1$	
	Met $\chi 1$	
CX-2C-2C-C	Glh $\chi 2$	C_α-C_β-C_γ-C_δ
	Gln $\chi 2$	
2C-2C-C-OH	Glh $\chi 3$	C_β-C_γ-C_δ-$O_{\epsilon 2}$
2C-2C-C-N	Gln $\chi 3$	C_β-C_γ-C_δ-$N_{\epsilon 2}$
CX-2C-2C-CO	Glu $\chi 2$	C_α-C_β-C_γ-C_δ
2C-2C-C-O2	Glu $\chi 3$	C_β-C_γ-C_δ-$O_{\epsilon 1}$
		C_β-C_γ-C_δ-$O_{\epsilon 2}$
CX-2C-2C-S	Met $\chi 2$	C_α-C_β-C_γ-S_δ
2C-2C-S-CT	Met $\chi 3$	C_β-C_γ-S_δ-C_ϵ

Table S3: Objective values O for each of the solving groups

Solving group	Amino acids	O_{ff99SB}	O_{ff14SB}	# params	# structures	# pairs
0	Cyx	1.5	1.2	20	1548	784 494
1	Glh Gln Glu Met	1.6	1.1	39	2986	587 699
2	Ile Thr Val	1.2	0.8	52	1368	210 564
3	Ash Asn	2.0	1.1	25	1800	435 852
4	Hid Hie Hip	1.3	1.0	24	1944	313 956
5	Phe Tyr	1.7	0.8	20	1224	187 308
6	Arg Lys	1.5	1.1	28	1656	345 531
7	Cys	1.3	1.0	16	648	104 652
8	Trp	1.3	1.0	20	648	104 652
9	Asp	2.5	0.9	16	648	104 652
10	Leu	1.2	0.9	16	648	104 652
11	Ser	1.4	0.9	16	648	104 652

Table S4: Distribution of REEs in terms of mean, standard deviation (stdev), minimum (min), and maximum (max), for ff99SB or ff14SB side chain parameters, against the conformations of each amino acid (AA) and backbone conformation (BB). '# confs' is the number of conformations in each set.

			ff99SB				ff14SB			
AA	BB	# confs	mean	stdev	min	max	mean	stdev	min	max
Arg	α	396	1.41	1.07	0.00	6.97	1.06	0.86	0.00	7.87
Arg	β	355	1.50	1.23	0.00	8.71	1.06	0.96	0.00	8.10
Ash	α	576	1.87	1.44	0.00	10.51	1.22	0.96	0.00	7.76
Ash	β	576	2.06	1.55	0.00	10.71	0.96	0.78	0.00	7.21
Asn	α	324	1.99	1.50	0.00	8.70	1.06	0.79	0.00	4.86
Asn	β	324	1.97	1.44	0.00	9.02	0.97	0.73	0.00	4.62
Asp	α	324	2.63	1.95	0.00	10.65	1.11	0.85	0.00	4.63
Asp	β	324	2.46	1.76	0.00	8.76	0.73	0.68	0.00	4.43
Cys	α	324	1.42	1.17	0.00	7.11	1.14	1.02	0.00	5.43
Cys	β	324	1.15	0.84	0.00	5.14	0.91	0.68	0.00	3.95
Glh	α	436	1.63	1.25	0.00	9.29	1.23	1.01	0.00	7.53

AA	BB	# confs	ff99SB				ff14SB			
			mean	stdev	min	max	mean	stdev	min	max
Glh	β	420	1.48	1.11	0.00	7.14	0.92	0.73	0.00	4.88
Gln	α	313	1.69	1.30	0.00	8.18	1.23	0.92	0.00	6.49
Gln	β	282	1.29	1.03	0.00	7.01	0.91	0.70	0.00	4.52
Glu	α	284	1.96	1.48	0.00	7.62	1.26	0.97	0.00	5.95
Glu	β	271	2.03	1.52	0.00	8.40	1.29	1.00	0.00	6.31
Hid	α	324	1.09	0.83	0.00	5.52	0.76	0.56	0.00	3.71
Hid	β	324	1.24	0.99	0.00	6.66	0.79	0.65	0.00	4.14
Hie	α	324	1.24	0.99	0.00	7.51	0.92	0.69	0.00	4.52
Hie	β	324	1.37	1.00	0.00	6.11	0.99	0.72	0.00	3.98
Hip	α	324	1.55	1.18	0.00	6.24	1.46	1.08	0.00	6.24
Hip	β	324	1.36	1.03	0.00	7.02	1.04	0.82	0.00	6.45
Ile	α	324	1.64	1.20	0.00	6.60	0.97	0.73	0.00	4.62
Ile	β	324	1.17	0.87	0.00	5.40	0.77	0.58	0.00	3.42
Leu	α	324	1.19	0.87	0.00	4.86	1.01	0.78	0.00	4.45
Leu	β	324	1.28	0.93	0.00	4.87	0.76	0.56	0.00	3.30
Lys	α	466	1.66	1.34	0.00	8.07	1.30	1.08	0.00	7.80
Lys	β	439	1.38	1.09	0.00	8.07	0.96	0.79	0.00	6.17
Met	α	483	1.33	1.10	0.00	8.01	1.16	0.96	0.00	7.30
Met	β	497	1.22	1.01	0.00	7.96	1.02	0.85	0.00	6.82
Phe	α	324	0.86	0.70	0.00	4.47	0.88	0.67	0.00	4.24
Phe	β	324	0.98	0.75	0.00	4.08	0.77	0.60	0.00	3.56
Ser	α	324	1.68	1.26	0.00	7.67	1.01	0.75	0.00	4.50
Ser	β	324	1.17	0.88	0.00	5.00	0.71	0.53	0.00	3.04
Thr	α	324	1.58	1.16	0.00	6.37	0.92	0.73	0.00	4.14

AA	BB	# confs	ff99SB				ff14SB			
			mean	stdev	min	max	mean	stdev	min	max
Thr	β	324	1.22	0.89	0.00	5.00	0.81	0.63	0.00	3.51
Trp	α	324	1.37	1.15	0.00	9.76	1.13	1.12	0.00	11.54
Trp	β	324	1.25	1.02	0.00	8.26	0.91	0.95	0.00	8.81
Tyr	α	288	2.44	1.92	0.00	8.63	0.83	0.62	0.00	3.82
Tyr	β	288	2.45	1.92	0.00	8.85	0.73	0.55	0.00	3.43
Val	α	36	1.17	0.86	0.00	3.37	0.77	0.58	0.00	2.77
Val	β	36	0.53	0.37	0.00	1.44	0.36	0.32	0.00	1.08

Alanine dipeptide PMFs

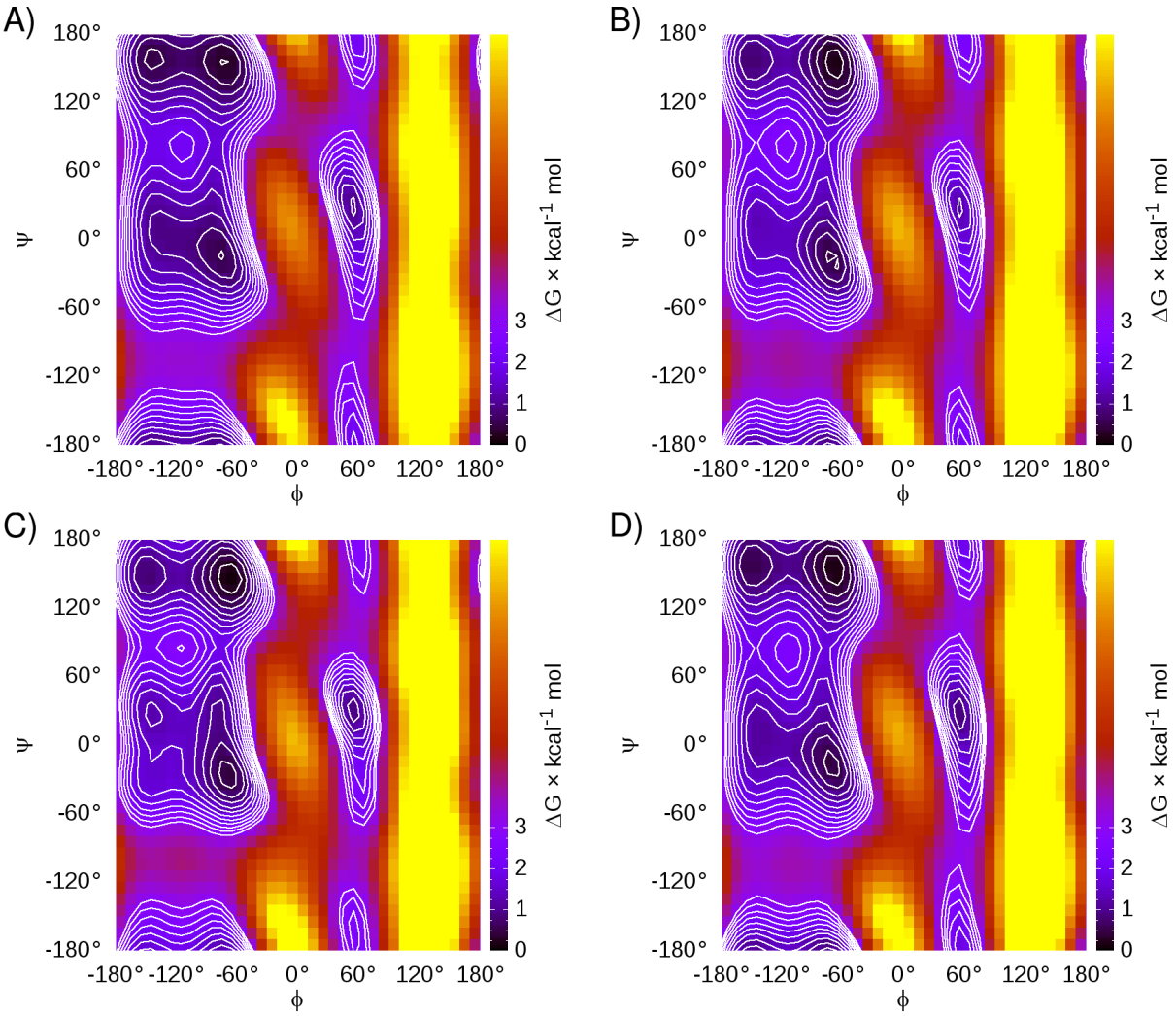

Figure S1: PMFs of alanine dipeptide in TIP3P water simulated with A) ff99SB, B) mod1ϕ, C) mod1ϕ2ψ, and D) mod3ϕ.

Defining E_{QM} and E_{MM}

Ideally, one should start with relatively close agreement between ff99SB and MP2/6-31+G**//HF/6-31G* energies (low AAE), with similar errors between different backbone conformations (low BBD), if dihedral parameters are to reconcile errors without explicit coupling to the backbone conformation. According to the penultimate rotamer library[7], the side chains of aspartate and asparagine depend most on backbone conformation; we thus chose them for initial testing of how the energy calculations impact coupling

between side chain and backbone dihedral parameters.

Restraining all backbone dihedrals and re-optimizing the QM structure with MM before calculating energy yielded both the lowest AAE ($2.55 \pm 0.09\,\mathrm{kcal\,mol^{-1}}$ for Asp and $1.98 \pm 0.01\,\mathrm{kcal\,mol^{-1}}$ for Asn, error bars reflect difference between α and β backbone context) and lowest BBD ($1.35 \pm 0.01\,\mathrm{kcal\,mol^{-1}}$ for Asp and $1.42 \pm 0.03\,\mathrm{kcal\,mol^{-1}}$ for Asn, error bars reflect difference between two staggered halves of structures), as shown in Figure S2 on the following page. At the opposite extreme, restraining just ϕ and ψ and using the QM structures to calculate MM energies resulted in the greatest AAE (3.45 ± 0.13 kcal mol^{-1} for Asp and 3.09 ± 0.74 kcal mol^{-1} for Asn) and BBD ($2.23 \pm 0.02\,\mathrm{kcal\,mol^{-1}}$ for Asp and $3.90 \pm 0.08\,\mathrm{kcal\,mol^{-1}}$ for Asn). Fundamental differences in the modeling of bonded and non-bonded interactions between QM and MM are likely exacerbated when the QM-optimized structures are evaluated in MM without re-optimization; these differences manifest as larger errors in MM energy, as well as less transferability between backbone contexts. Restraining all possible combinations of four-atoms describing each dihedral in both the backbone and side chain was also attempted (this approach led to the ff12SB parameter set, see Section on page 42), but restraining all 4-atom dihedrals in the side chains prevented relaxation of angle terms in MM optimization, leading to increased error that likely would not be present in a simulation when steric clashes can be alleviated through adjustment of covalent structure. Based on these results, we made the decision to restrain all backbone dihedrals during structure optimization, but only the defining dihedrals for side chains, and to re-optimize the QM structures with the MM model (using the same restraints) prior to calculation of MM energies. These energies were used in the calculation of the objective function in Equation (6).

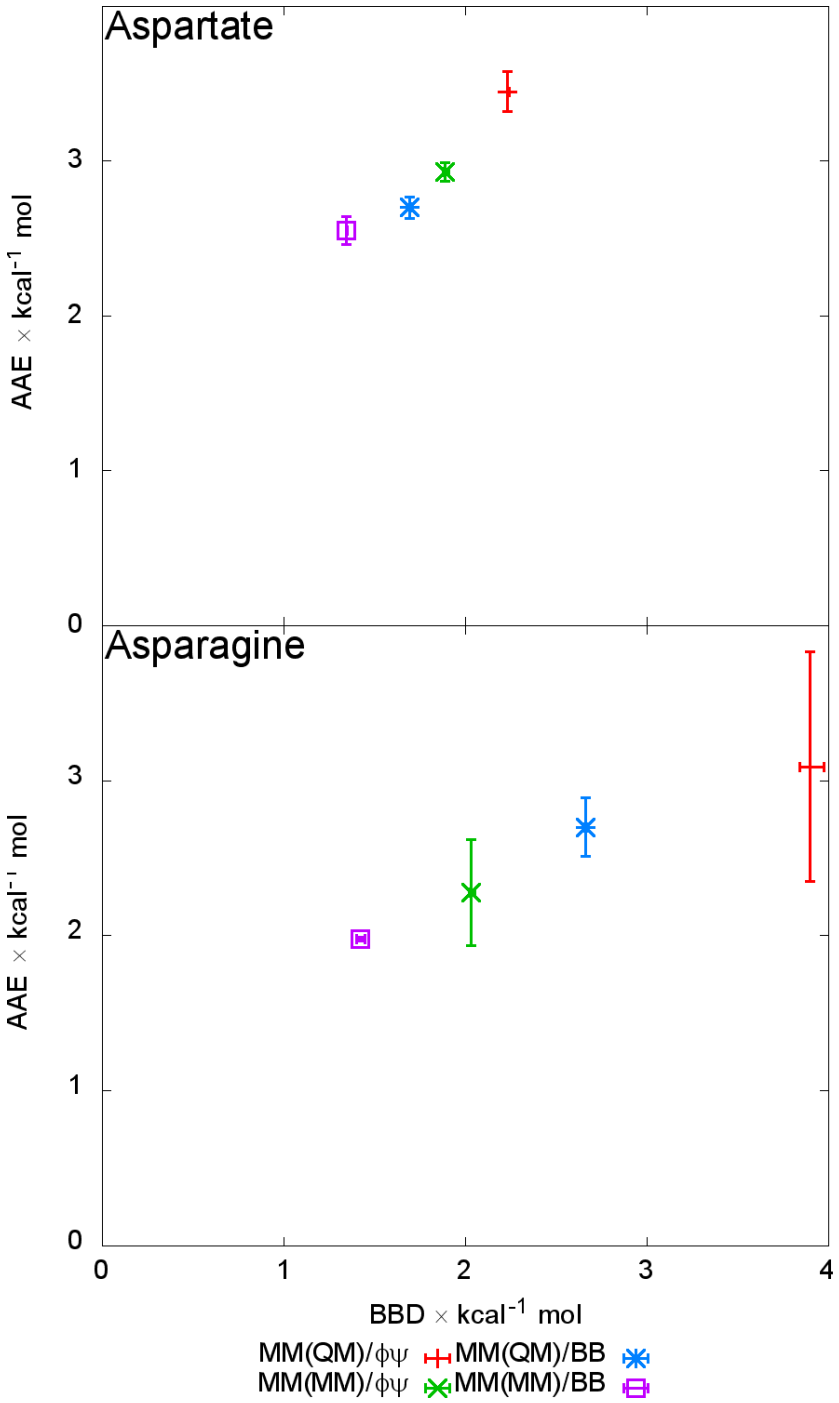

Figure S2: AAE vs. BBD of aspartate and asparagine, calculating MM energies of QM structures and restraining: ϕ and ψ (red crosses) or all backbone dihedrals (blue stars); or calculating MM energies of MM re-optimized structures and restraining: ϕ and ψ (green 'X's) or all backbone dihedrals (purple squares). The latter provides the lowest AAE values, as well as the best intrinsic transferability between backbone conformations. Error bars in AAE indicate difference between AAE calculated in the α or β backbone context, and BBD using half of the structures.

Backbone modification

We changed the backbone potential to enhance helical sampling and scalar couplings[8] in Ala_5. To be sure we corrected the appropriate backbone potential or combination of backbone potentials, we perturbed ϕ and ψ backbone potentials and then combined all pairs of ϕ and ψ potentials.

Modifications to ϕ potentials targeted both scalar coupling deviations and helical sampling. Too high HN-H scalar couplings suggest too many structures near $\phi = -120°$, where this scalar coupling is maximal. This transition was destabilized by increasing the $n = 3$ ϕ' amplitude from 0.4 kcal/mol to 0.6 kcal/mol or 0.8 kcal/mol, modifications (mods) referred to as 3ϕ and 4ϕ, respectively. Not enough helical content, particularly ppII, also suggests that helices are not stable enough relative to strands. Helices were stabilized by decreasing the $n = 2$ ϕ' amplitude from 2 kcal/mol to 1.8 kcal/mol, yielding mod1ϕ and 2ϕ when added to mod3ϕ and 4ϕ, respectively.

As another work suggested that helical undersampling results from errors in ψ, not ϕ, we also explored several ψ corrections. Two simply stabilize α relative to β and ppII. The first stabilizes ψ in the vicinity of $-45°$ to $-40°$ by increasing the ψ' $n = 1$ amplitude from 0.2 kcal/mol to 0.3 kcal/mol and phase shifting by $-60°$, denoted by 4ψ. The second favors structures centered on the eclipsed ψ of 0° by increasing the $n = 1$ ψ amplitude from 0.45 kcal/mol to 0.6 kcal/mol or 0.7 kcal/mol, the former of which constitutes modification 3ψ. Modification 2ψ was formed from mod3ψ by making structures centered around ψ of $\pm 45°$ and $\pm 135°$ more favorable by introducing a ψ' $n = 4$ term with amplitude 0.4 kcal/mol and phase shift of 120°. Starting with this change together with the 0.7 kcal/mol amplitude variation of the second basic ψ correction, we stabilized structures near ψ of $-30°$ and 150° and destabilized structures near $-120°$ and 60°, increasing the barriers, by increasing the ψ' $n = 2$ amplitude from 0.2 kcal/mol to 0.5 kcal/mol, this conglomerate referred to as mod1ψ.

Each of the ϕ variants was then combined with each of the ψ variants, including ff99SB ϕ and ψ corrections. Thus we formed 24 ff99SB variants to evaluate which works best.

Table S5: Revisions to ϕ'

	Correction term		
Force field	$V1'/2$	$V2'/2$	$V3'/2$
ff99SB	2.0	2.0	0.4
mod1φ	2.0	1.8	0.8
mod2φ	2.0	1.8	0.6
mod3φ	2.0	2.0	0.8
mod4φ	2.0	2.0	0.6
mod5φ	1.8	2.0	0.8

ff99SB and candidate changes to the ϕ' correction mod1-5φ. Phase shift is 0°. Parameters changed from ff99SB are colored blue.

Table S6: Revisions to $\psi(')$

	Force field				
Correction term	ff99SB	mod1ψ	mod2ψ	mod3ψ	mod4ψ
$V1/2$	-0.45	-0.70	-0.60	-0.60	-0.45
$V2/2$	-1.58	-1.58	-1.58	-1.58	-1.58
$V3/2$	-0.55	-0.55	-0.55	-0.55	-0.55
$V1'/2$	0.20	0.20	0.20	0.20	0.30[a]
$V2'/2$	0.20	0.50	0.20	0.20	0.20
$V3'/2$	0.40	0.40	0.40	0.40	0.40
$V4'/2$	0	0.40[b]	0.40[b]	0	0

a. Phase shift of $-60°$

b. Phase shift of 120°

ff99SB and candidate changes to ψ and ψ' corrections. Negative amplitude indicates phase shift of 180°. The mod4ψ ψ' $n = 1$ correction has a phase shift of $-60°$. The mod1ψ and mod2ψ ψ' $n = 4$ corrections have a phase shift of 120°. Parameters changed from ff99SB are colored blue.

Building hydrogen bond surrogate peptide

We restrained the hydrogen bond between the Ac1:CO and the A5:HN. Two criteria were used to identify an appropriate Ac1:O - A5:HN restraint distance. First, the PDB was surveyed for proteins whose structure was determined by X-ray crystallography at a resolution of <0.9 Å, to provide hydrogen atom positions. Next, we looked at those proteins which had an α-helix length of 40–50 amino acids so that a large number of backbone helical hydrogen bonds would be present. One suitable structure was found satisfying these two criteria, *Pichia pastoris* aquaporin Aqy1 (PDB ID: 3ZOJ),[9] which was resolved at 0.88 Å and had 106 backbone helical hydrogen bonds. We histogrammed the length of all the backbone α-helical hydrogen bonds. The peak of the histogram of these distances was observed at 2.03 Å. To find the optimal weight for restraining the Ac1:O - A5:HN bond distance, test simulations were run for 160.0 ns using ff99SB[10] using different weights and the histogram of the Ac1:O - A5:HN distance was plotted (Figure S3 on the following page). Using a restraint weight of 100.0 kcal/mol/Å^2 provides a peak at 2.03 Å with similar distribution to that found in 3ZOJ, and hence, was used for production runs. The authors note that the distribution is likely narrower for a crystal structure than expected from room-temperature dynamics; as the goal is to emulate a covalent bond, referring to a crystal structure may be reasonable.

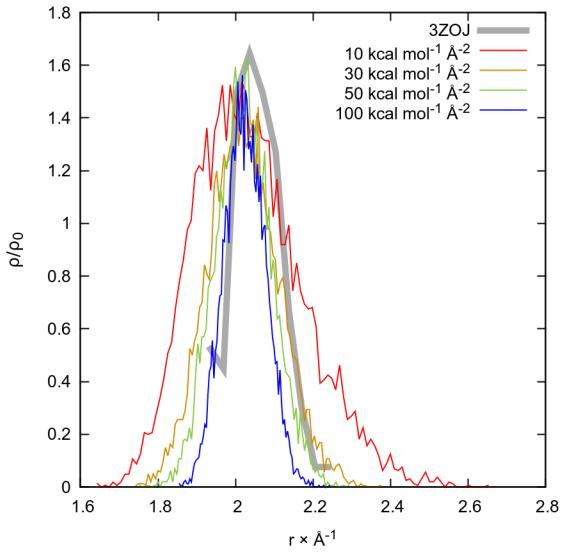

Figure S3: The Ac1:O - A5:HN distance probability distribution using different weights. The units of the weights are in kcal/mol/Å^2. The distribution of hydrogen bond distances observed in 3ZOJ is shown in gray.

Additional testing analysis

K19 per-residue helicity analysis

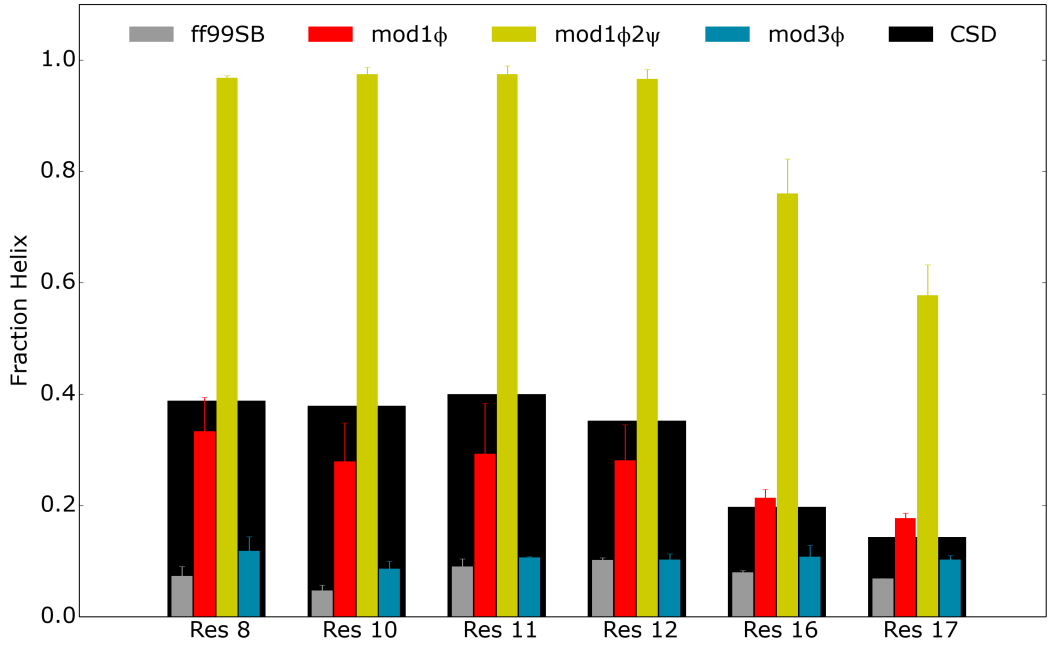

Figure S4: The helicity of each residue in K19, according to ff99SB (gray), mod1ϕ (red), mod1ϕ2ψ, mod3ϕ, and CSDs[11] (black). The force field helicity was determined from ϕ/ψ angles, as described in the Methods section of the main text. The mod1ϕ simulations are in best agreement with experimental CSDs.[11]

CLN025

Table S7: Sum of the NOE violations from the restraints determined in Ref 12 for CLN025, for each simulation using ff14SB and ff99SB starting from linear and native conformations. *FF=force field

run / FF*	linear				native			
	1	2	3	4	1	2	3	4
ff14SB	3.6	1.8	3.7	2.4	2.1	1.8	1.5	2.1
ff99SB	2.4	3.8	3.3	2.7	3.3	1.8	2.5	4.9

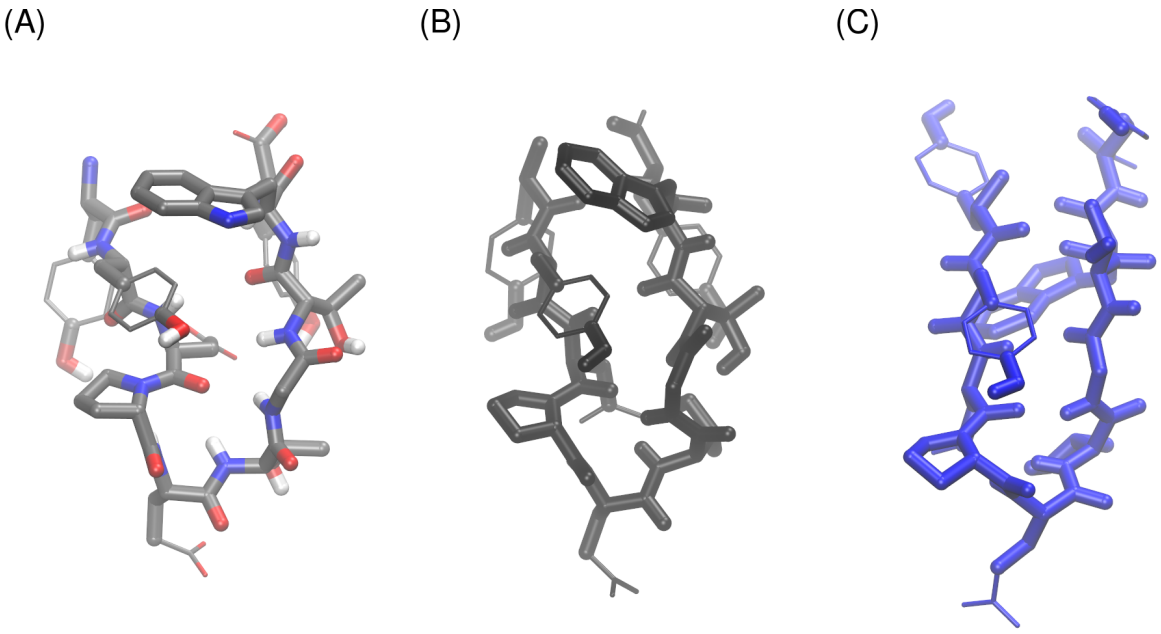

Figure S5: Licorice structures of CLN025. The NMR structure closest to the ensemble average,[12] colored by atom (A); the centroid of cluster 0, the native-like cluster, colored black (B); the centroid of cluster 1, where a shift in hydrogen bonding accompanies extension of the C-terminus of the second strand past the N-terminus of the first strand and flipping of W9 to the opposite side of the hairpin from Y2, against which it stacks in the NMR structure and cluster 0, and P4, which stacks against Y2, colored blue (C). Large licorice indicates atoms used in the clustering mask; smaller licorice atoms were omitted from clustering.

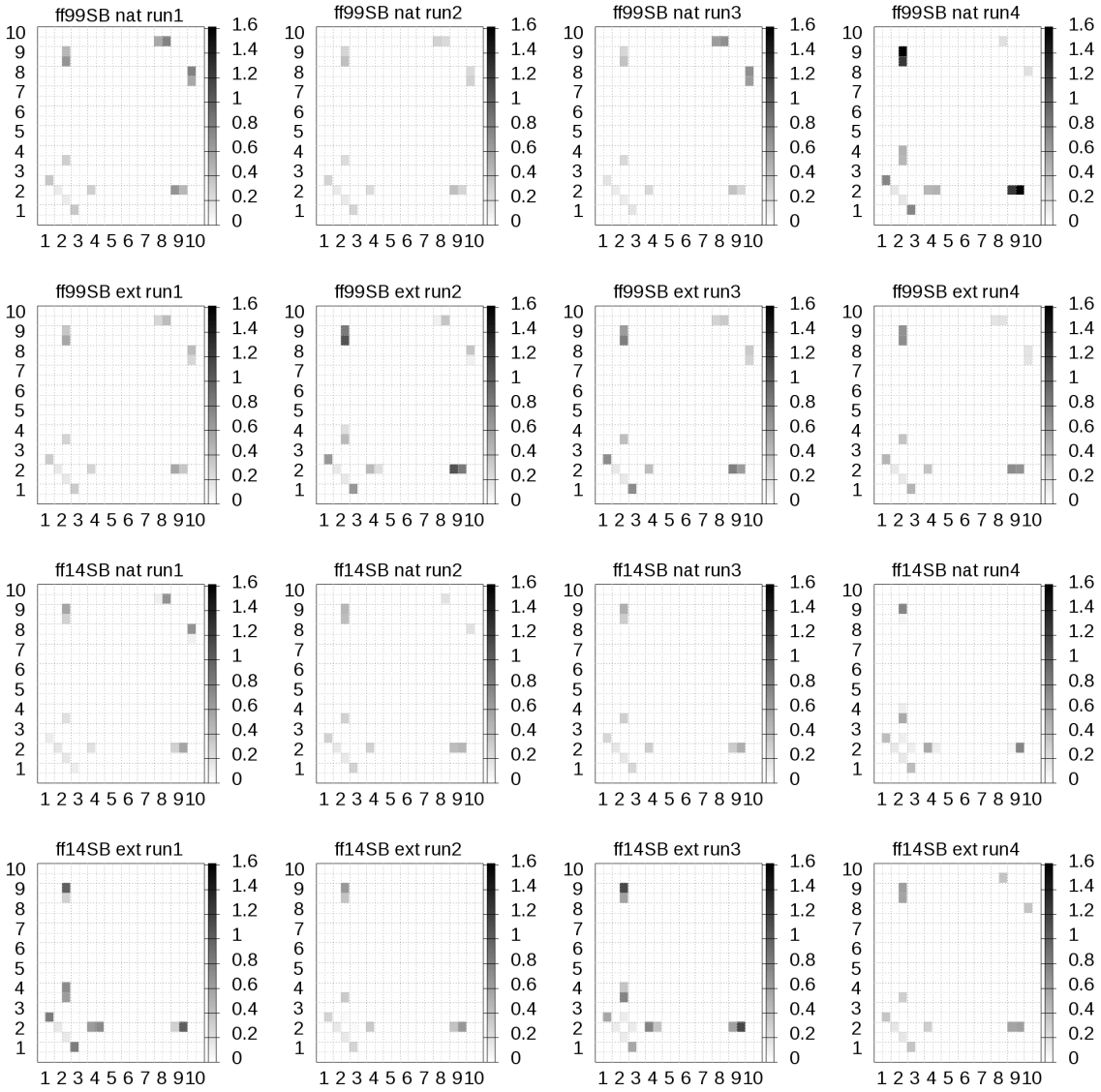

Figure S6: NOE[12] violations of CLN025 simulations with ff99SB and ff14SB, of each amino acid backbone and side chain to each other amino acid backbone and side chain. Nearly all simulations have minor violations within the N-terminus and between the N- and C-termini, whereas ff99SB simulations have greater violations within the C-terminus than ff14SB.

Protein backbone RMSDs

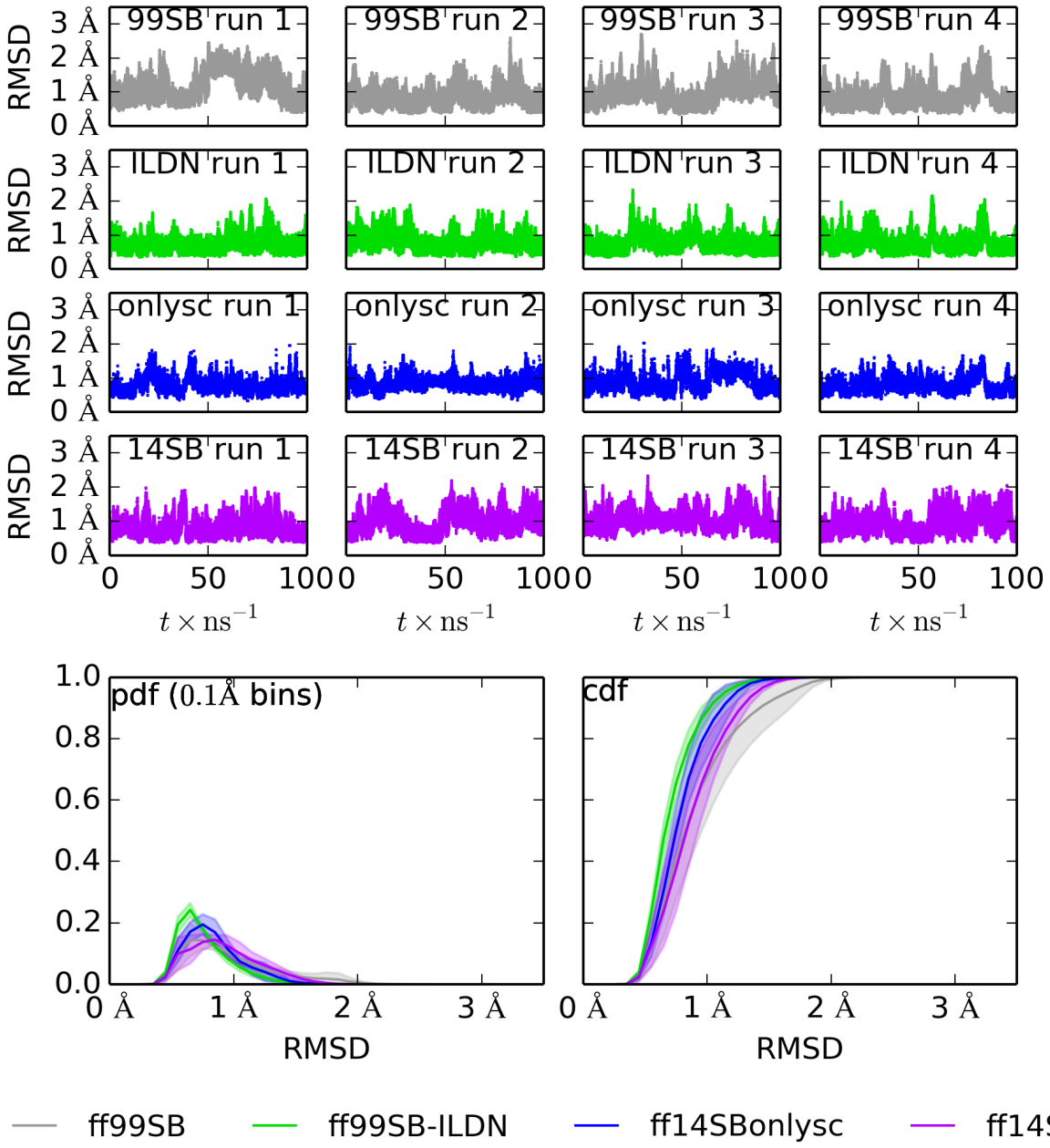

Figure S7: GB3 backbone (N, Cα, C) RMSD to 1P7E[13] for four runs of ff99SB (top row), ff99SB-ILDN (second row), ff14SBonlysc (third row), and ff14SB (fourth row). The probability density function (pdf) and cumulative distribution function (cdf) are plotted for each force field in the bottom row.

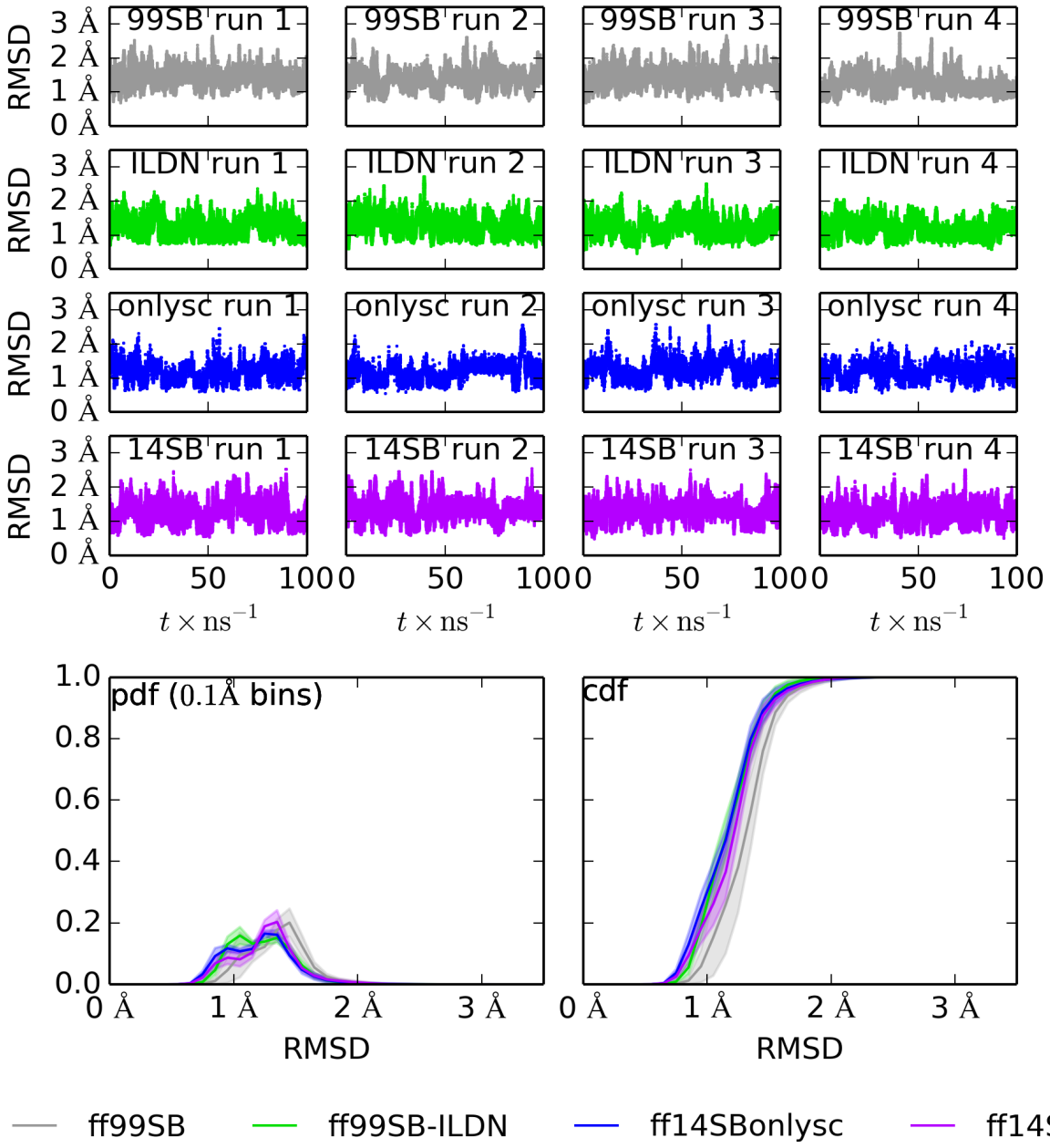

Figure S8: BPTI backbone (N, Cα, C) RMSD to 5PTI[14] for four runs of ff99SB (top row), ff99SB-ILDN (second row), ff14SBonlysc (third row), and ff14SB (fourth row). The probability density function (pdf) and cumulative distribution function (cdf) are plotted for each force field in the bottom row.

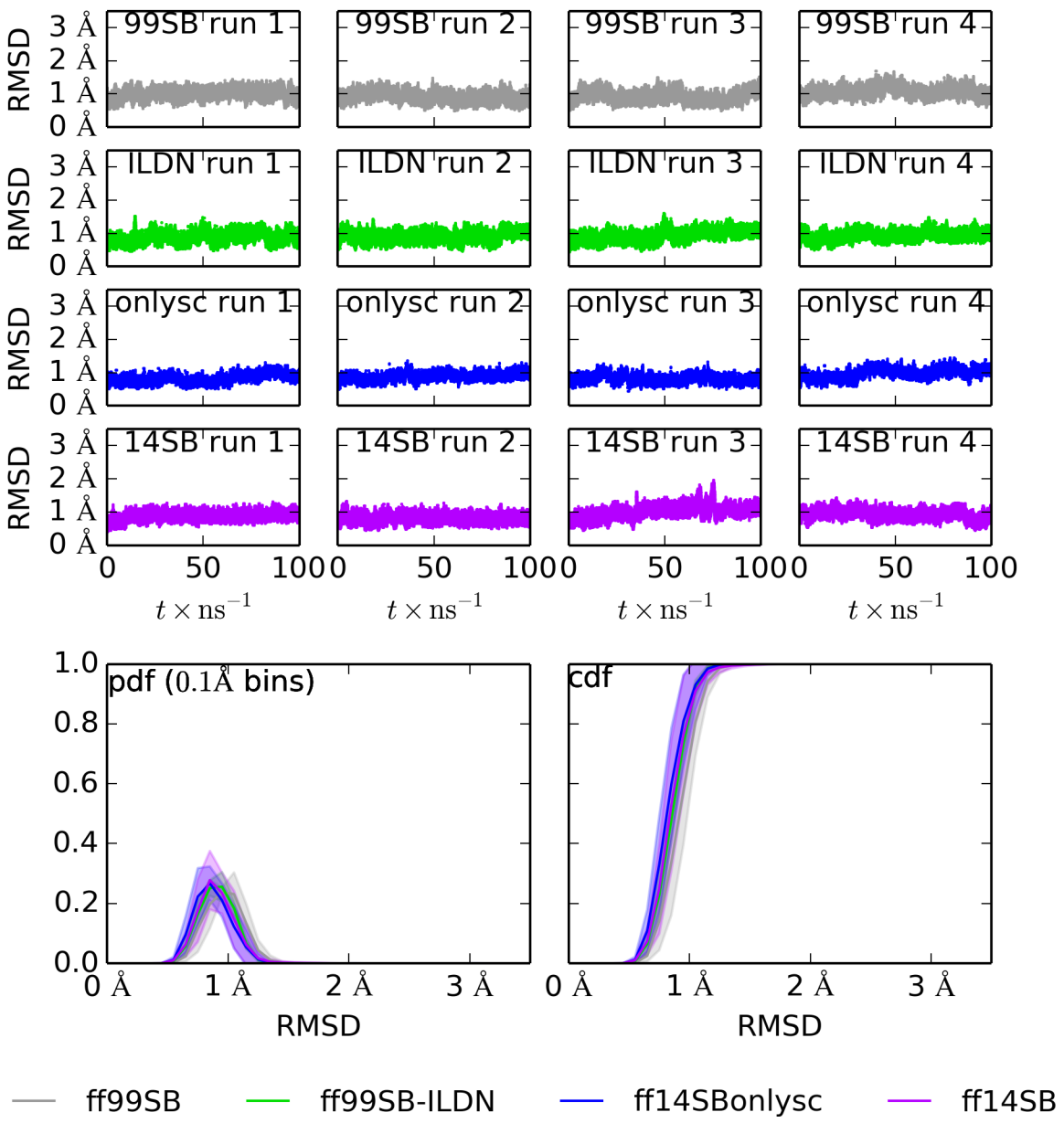

Figure S9: Ubiquitin backbone (N, Cα, C) RMSD to 1UBQ[15] for four runs of ff99SB (top row), ff99SB-ILDN (second row), ff14SBonlysc (third row), and ff14SB (fourth row). The probability density function (pdf) and cumulative distribution function (cdf) are plotted for each force field in the bottom row.

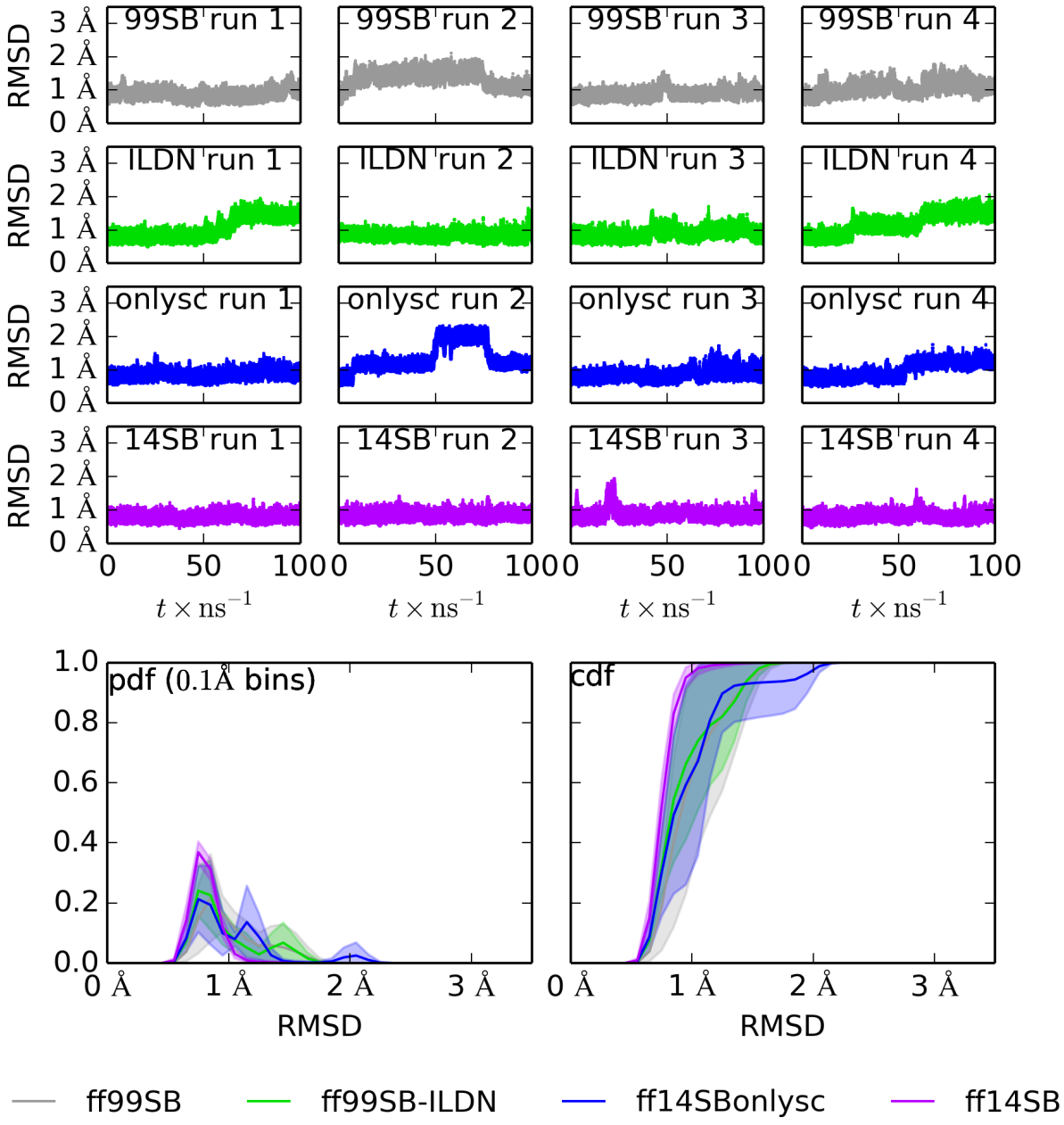

Figure S10: Lysozyme backbone (N, Cα, C) RMSD to 6LYT[16] for four runs of ff99SB (top row), ff99SB-ILDN (second row), ff14SBonlysc (third row), and ff14SB (fourth row). The probability density function (pdf) and cumulative distribution function (cdf) are plotted for each force field in the bottom row.

Protein ramachandran histograms

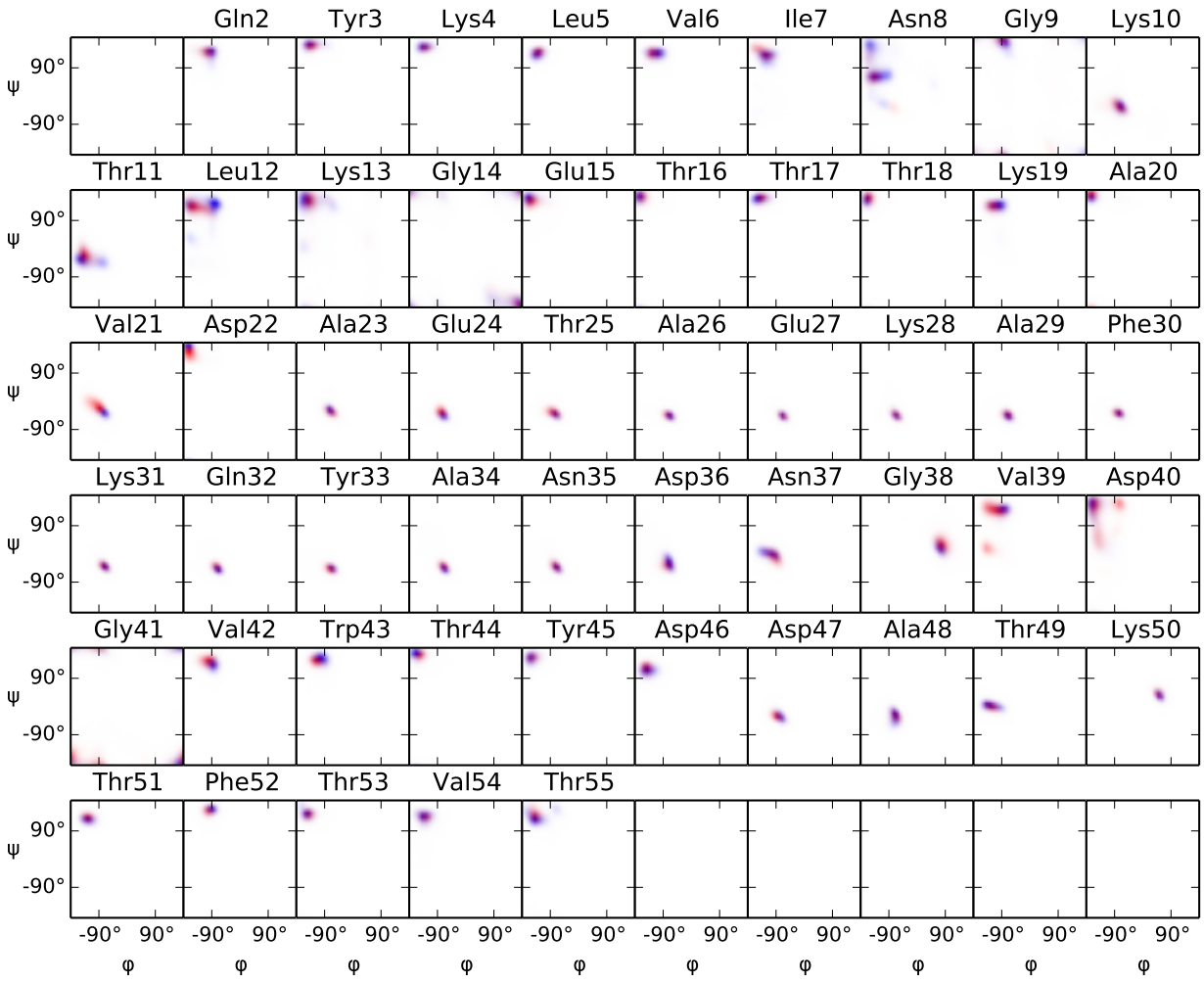

Figure S11: Ramachandran histograms of each residue in GB3 from four simulations each with ff99SB (red) and ff14SB (blue)

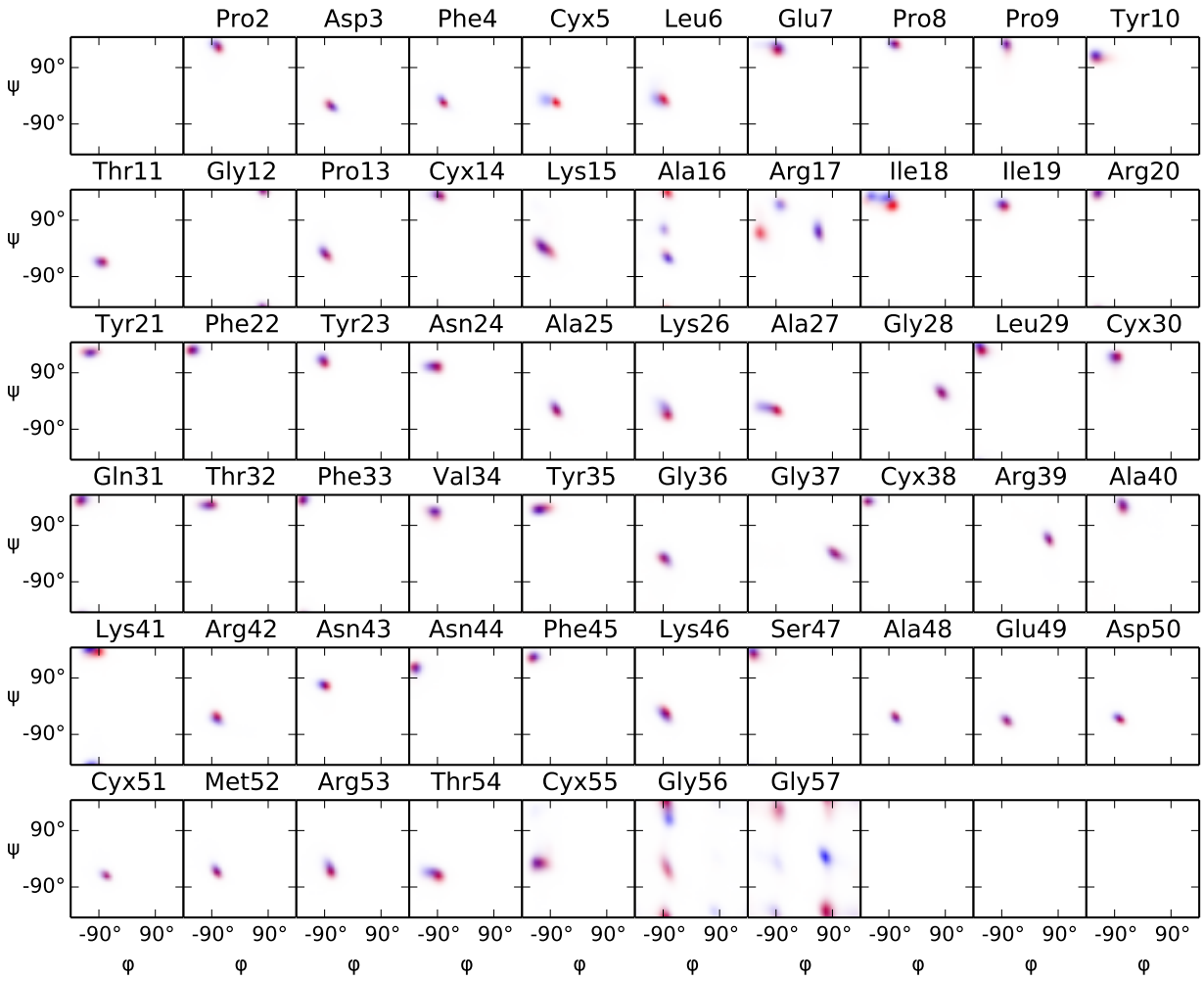

Figure S12: Ramachandran histograms of each residue in bovine pancreatic trypsin inhibitor from four simulations each with ff99SB (red) and ff14SB (blue)

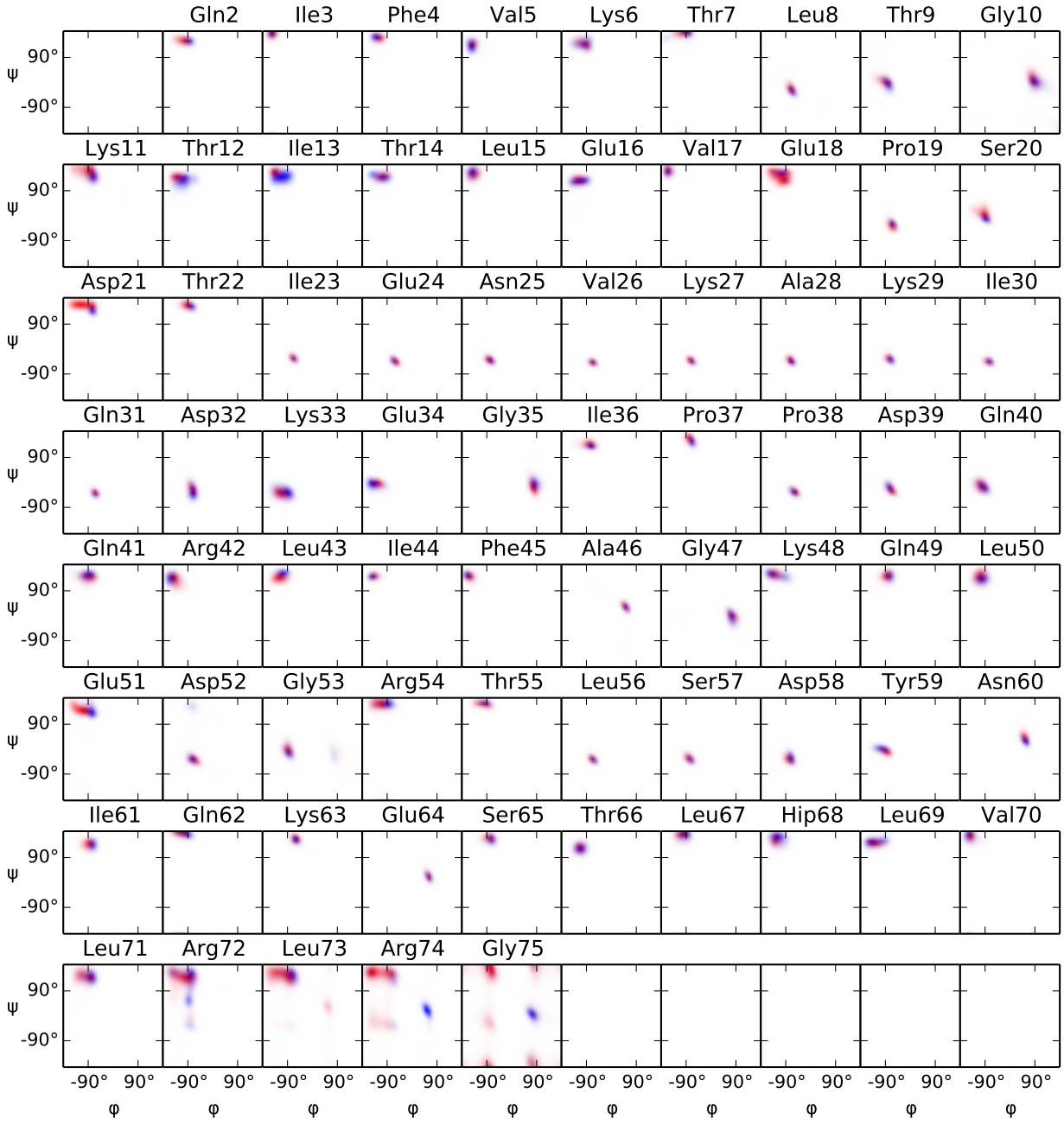

Figure S13: Ramachandran histograms of each residue in ubiquitin from four simulations each with ff99SB (red) and ff14SB (blue)

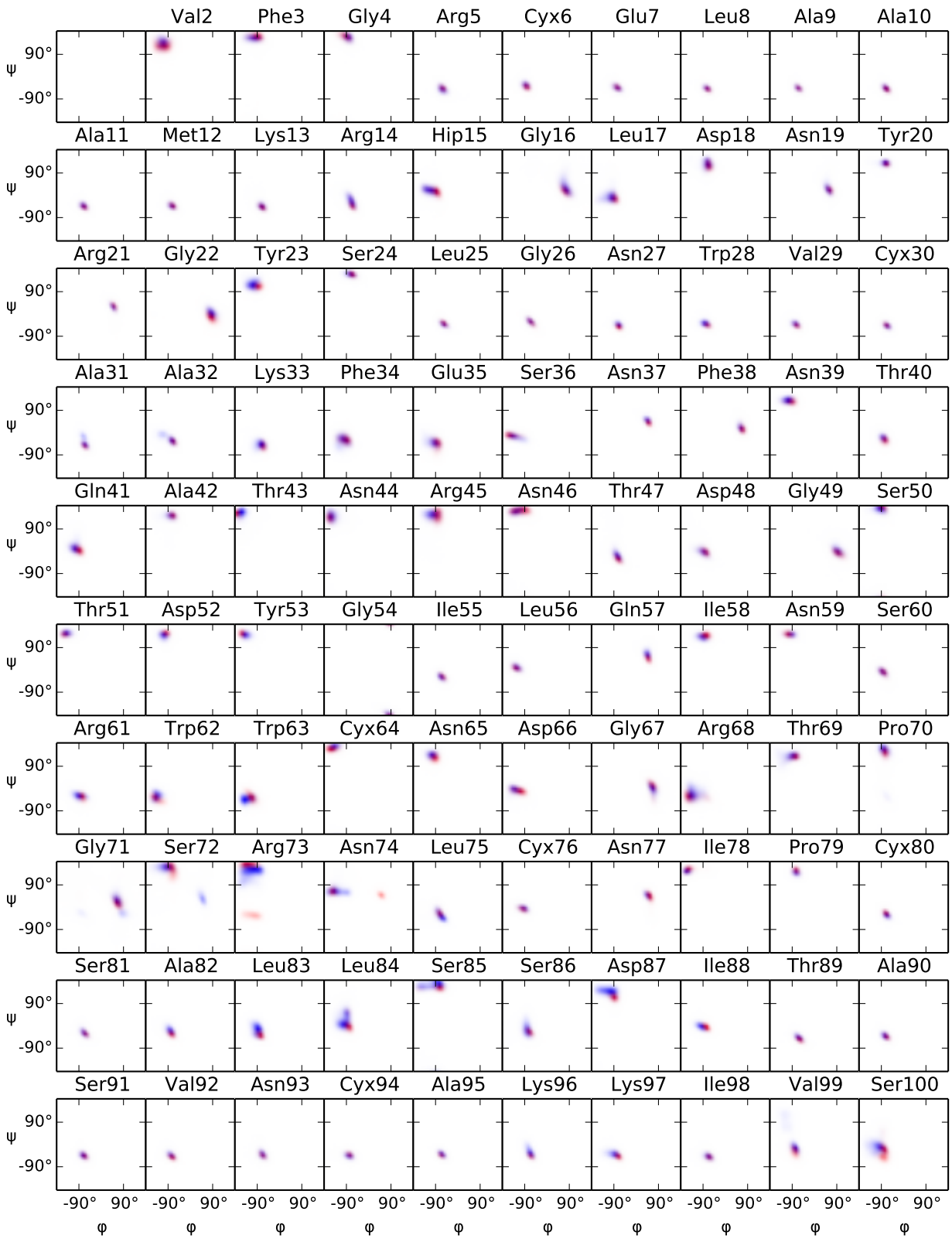

Figure S14: Ramachandran histograms of each residue in lysozyme from four simulations each with ff99SB (red) and ff14SB (blue), for residues 2 to 100.

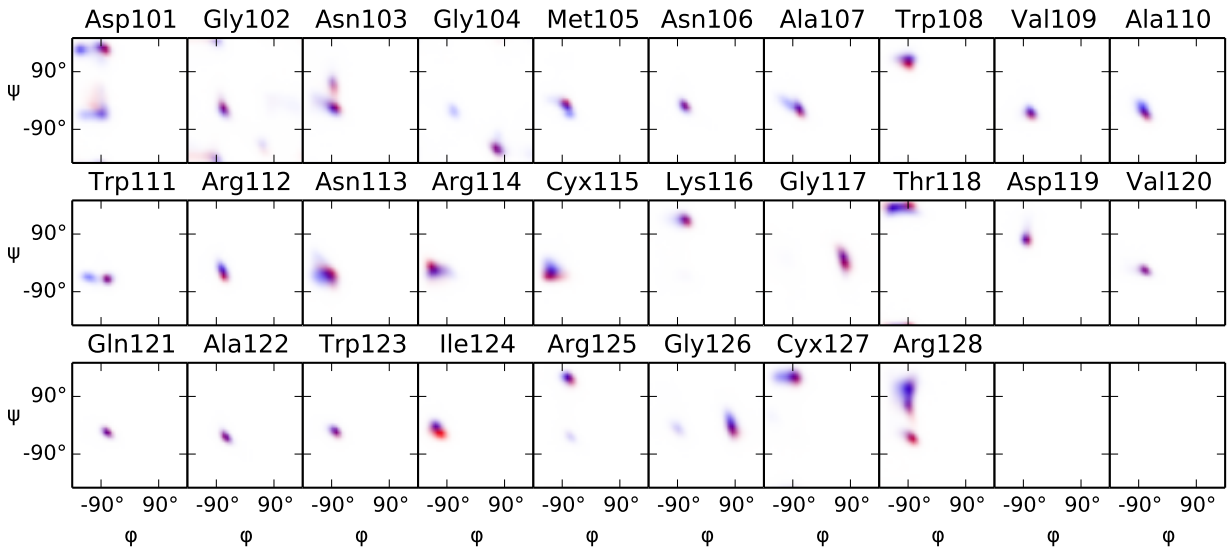

Figure S15: Ramachandran histograms of each residue in lysozyme from four simulations each with ff99SB (red) and ff14SB (blue), for residues 101 to 128.

Significance analysis

One way to incorporate statistical significance into analyzing force field differences is to plot the average difference in errors for all scalar couplings whose comparison satisfies any of a range of p-values. Those that satisfy lower p-values may be considered more informative than those that only satisfy higher p-values. The probability that distributions are not different was approximated by Welch's t-test[17]. The p-value was calculated using the survival function of the SciPy[18,19] stats module, based on t as in Equation (2) with μ_{FF} and SE_{FF} corresponding to the average normalized error and standard error of the mean normalized error, respectively, for each force field FF, and degrees of freedom approximated by the Welch-Satterthwaite equation[17,20], (Equation (3); $n1$, being 3 for all force fields, enters the numerator).

$$t = \left(\mu_{\text{ff14SB}} - \mu_{\text{ff99SB-ILDN}}\right)\left(SE^2_{\text{ff14SB}} - SE^2_{\text{ff99SB-ILDN}}\right)^{-\frac{1}{2}} \tag{2}$$

$$d.f. = \frac{3\left(SE^2_{\text{ff14SB}} + SE^2_{\text{ff99SB-ILDN}}\right)^2)}{SE^4_{\text{ff14SB}} + SE^4_{\text{ff99SB-ILDN}}} \tag{3}$$

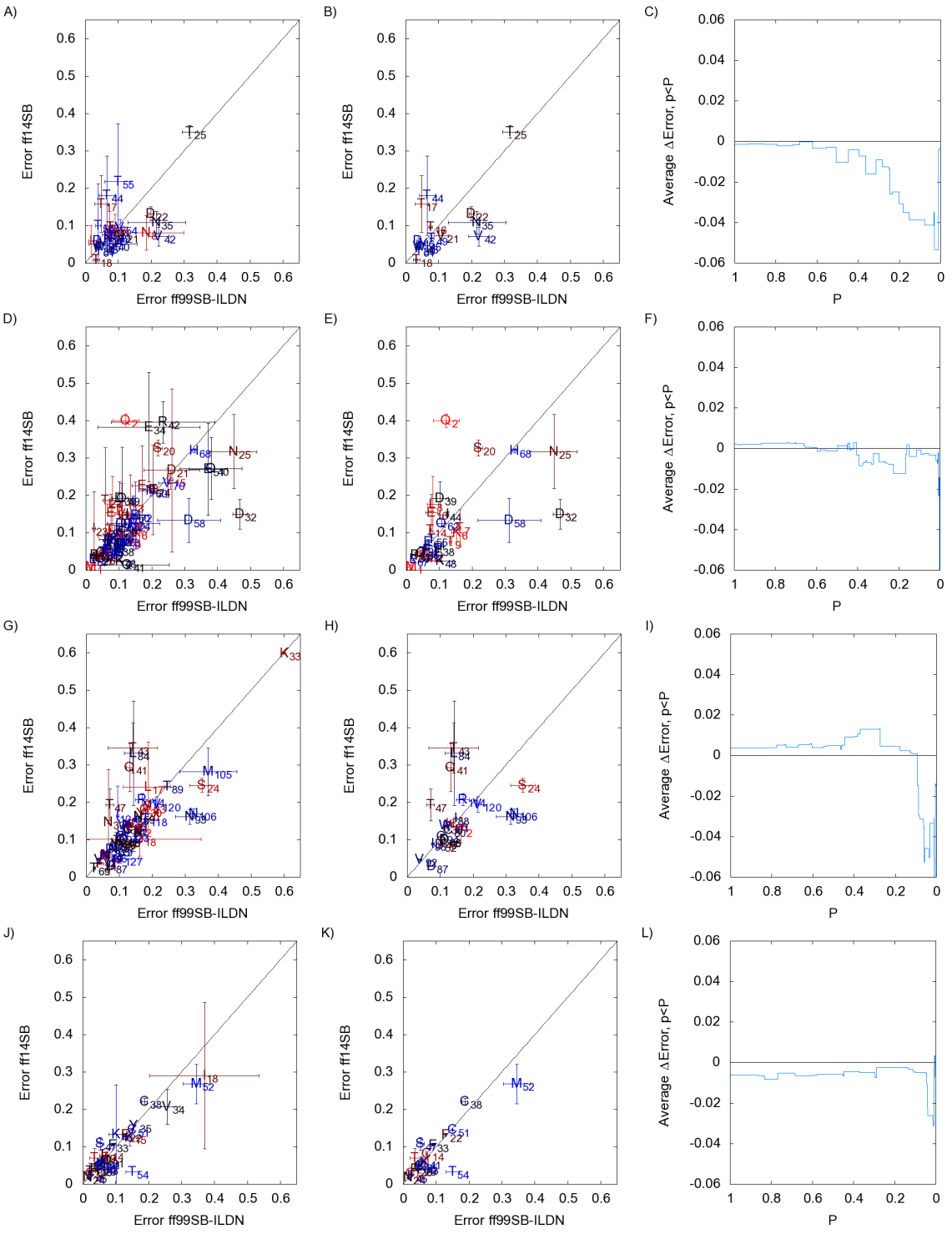

Figure S16: Left column: all average normalized errors (ANE, defined in main text) according to ff99SB-ILDN[21] (x-axis) and ff14SB (y-axis). Middle column: a subset of the errors where the uncertainties do not cross the equivalence line. Right column: the average difference in normalized error from ff99SB-ILDN to ff14SB (y-axis) for normalized errors with significance of $p < P$ (x-axis). Top row: GB3 (A-C). Second row: ubiquitin (D-F). Third row: lysozyme (G-I). Bottom row: BPTI (J-L).

Backbone dependence

As ubiquitin D32 was the most statistically different between the two force fields, we attempted to decompose its simulation accuracy according to fitting method, potentially providing insight to guide future parameter optimization efforts. First, we used ff14SB aspartate side chain parameters in ff99SB-ILDN to ensure that aspartate side chain parameters are responsible for observed differences. This significantly reduced the D32 ANE to a value comparable to ff14SB (0.077 ± 0.006), confirming direct influence of the Asp parameters on D32 dynamics. The most obvious methodological difference that could explain this phenomenon is the inclusion of helical backbone structures in training. We repeated the optimization for solving group 10 (containing just aspartate), but using only β backbone conformations in Equation (5). Simulations using these parameters still resulted in rather low ANE of 0.070 ± 0.008, suggesting that this particular improvement was not due to inclusion of fitting for both backbone conformations. A second possibility is that our fitting protocols had several differences compared to ff99SB-ILDN, such as weighting of squared QM-MM energy differences by QM energy in the ff99SB-ILDN fitting, which could introduce bias if positions of side chain rotamer minima are coupled to backbone conformation. Another protocol difference is that ff14SB parameters used two 4-atom dihedrals to describe $\chi 1$, while ff99SB-ILDN fit only one set. We refit parameters for solving group 10 using the ff14SB protocol but with the aspartate QM and MM energies published by Lindorff-Larsen et al.[21]. With the resulting parameters, sampling of D32 was not improved compared to ff99SB-ILDN (ANE $= 0.42 \pm 0.07$), suggesting that the D32 performance is related to differences in the QM benchmarks used to train the two force fields rather than the optimization protocol. Although both data sets used a 2D scan of $\chi 1$ and $\chi 2$, the resulting energies are influenced by the level of QM theory and the restraints used to generate potential energy surfaces for fitting. To test the influence of restraints, we used the potential energy surfaces that we generated with different structure optimization methods to test backbone-dependence (Figure 3). We therefore retrained solving group 10 parameters based on potential energy scans

of only β, or α and β conformations, using the combinations of restraints and QM or MM optimized structures as carried out for Figure S2 on page 19. The ANE of D32, and of all aspartates in ubiquitin, were plotted against the BBD of each method in Figure S17 on the following page. For the parameters trained using only β dipeptides, the BBD of each method forwardly predicts the error of D32 obtained using those parameters. This suggests that how the structures in a potential energy surface are generated can significantly alter their transferability. In fact, the combination matching ff99SB-ILDN (restraining only ϕ and ψ, using QM structures for MM energies) also provided comparable results to ff99SB-ILDN (ANE of 0.32 ± 0.11), suggesting that the deviation in MD from solvated protein NMR data can be traced to the restraint method used during parameter development. The largest errors arise when using QM structures for MM energies with fewer restraints; these errors are reduced when both α and β dipeptides are used in fitting, perhaps because artifacts from backbone interactions are lessened when requiring that the parameters work in multiple backbone contexts (for example, D32 ANE is reduced from 0.32 ± 0.11 with β-only training to 0.067 ± 0.007 using both α and β). Although we examined only one location in detail (D32), the same trend holds when considering all Asp residues in ubiquitin (Figure S17 on the next page). These results on agreement between MD and NMR also mirror the findings in Figure S2 on page 19, where the ability to reproduce QM energies (AAE) showed a similar dependence on BBD for different restraint methods. Taken together, the results show not only the sensitivity of the model to restraint method, but also reinforce that improved reproduction of gas-phase QM dipeptide energies leads to a better match to NMR data for proteins simulations in water.

If we expand the backbone-dependent comparison to consider all ILDN residues within helices versus all those without, we observe the same trends of ff14SB backbone-independence. The average errors of all I, L, D, and N residues in helices were 0.18 ± 0.01 with ff99SB-ILDN and 0.13 ± 0.01 with ff14SB. On the other hand, the average errors of all ILD and N residues not in helices were 0.11 ± 0.01 with both force fields. This indicates that overall

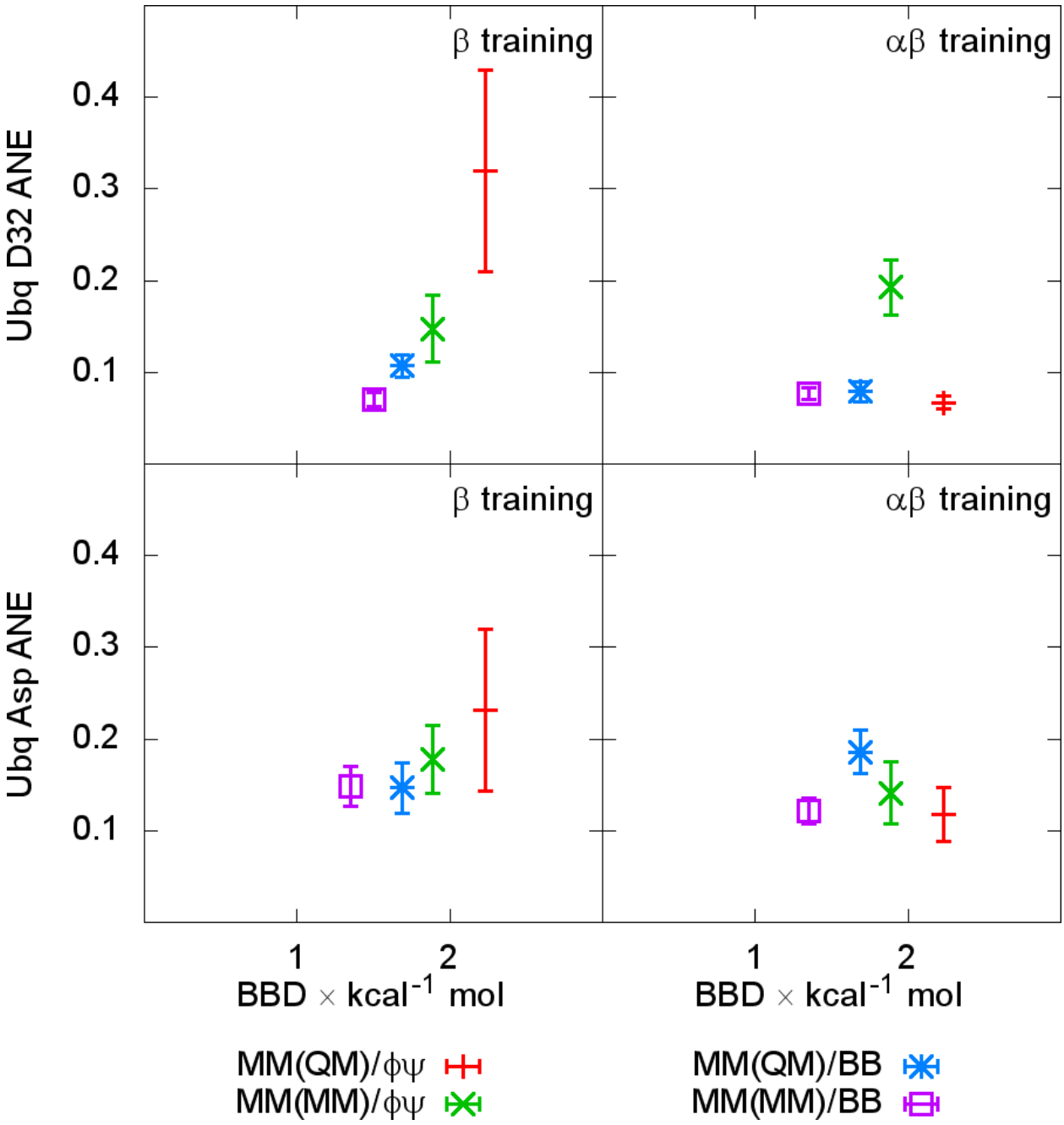

Figure S17: Simulated average normalized error (ANE) of ubiquitin (Ubq) D32 and all Ubq aspartate (Asp), with parameters developed from β or α and β conformations of aspartate dipeptides with restraints on all backbone dihedrals (BB) or only ϕ and ψ (ϕψ), and with molecular mechanics energies calculated for molecular mechanics structures (MM(MM)), or quantum mechanics structures (MM(QM)), versus backbone dependence on the x-axis. Parameters from β dipeptides with less backbone-dependent errors against quantum mechanics also exhibit lower errors against helical D32 scalar couplings. Training with α and β conformations performs comparably or, as in MM(QM)/ϕψ, better against scalar couplings.

errors for side chains in helical context are improved with ff14SB relative to ff99SB-ILDN, and that in ff14SB these errors are similar in magnitude to the non-helical side chain errors for both force fields. It seems reasonable to conclude that this improved transferability in ff14SB arises directly from the training of ff14SB against more transferable energy targets than other options tested, with multiple backbone conformations.

Order parameter calculations using 2, 4, and 8 ns windows

In addition to the order parameter calculations reported in the main text, we calculated order parameters for GB3, ubiqutin, and lysozyme using iRED[22] with 2, 4, and 8 ns windows, consistent with previous work by Li and Brüschweiler[23] (ubiquitin and lysozyme) and Markwick et al.[24] (GB3). According to this analysis, all force fields are within 0.05 RMSD of experimental S^2, with subtle differences between them.

Several turns or loops increased in order with ff14SB. In the cases of loops L1 and L4 in lysozyme, this increased order better reproduces experimental order parameters. Turn T3 in GB3 and loop L3 in lysozyme, however, may have become too ordered although the differences are within precision errors. L3 begins with S85, which is 0.16 ± 0.04 too ordered. With ff99SB, S85 was already 0.10 ± 0.02 too ordered, meanwhile D87 was 0.09 ± 0.02 too disordered with ff99SB but only 0.05 ± 0.01 too ordered with ff14SB. Naturally, these estimates depend on both the accuracy of the iRED method and the uncertainty in the simulations and experiments; absolute comparisons against the experimental S^2 differing by 0.06 ± 0.04 should not be overemphasized. But as a trend, there appears to be slightly less flexibility in loops in ff14SB compared to ff99SB, both aiding and lessening agreement between iRED and experimental order parameters. We conclude that ff14SB maintained ff99SB order parameter reproduction on average, but with subtle reduction in flexibility.

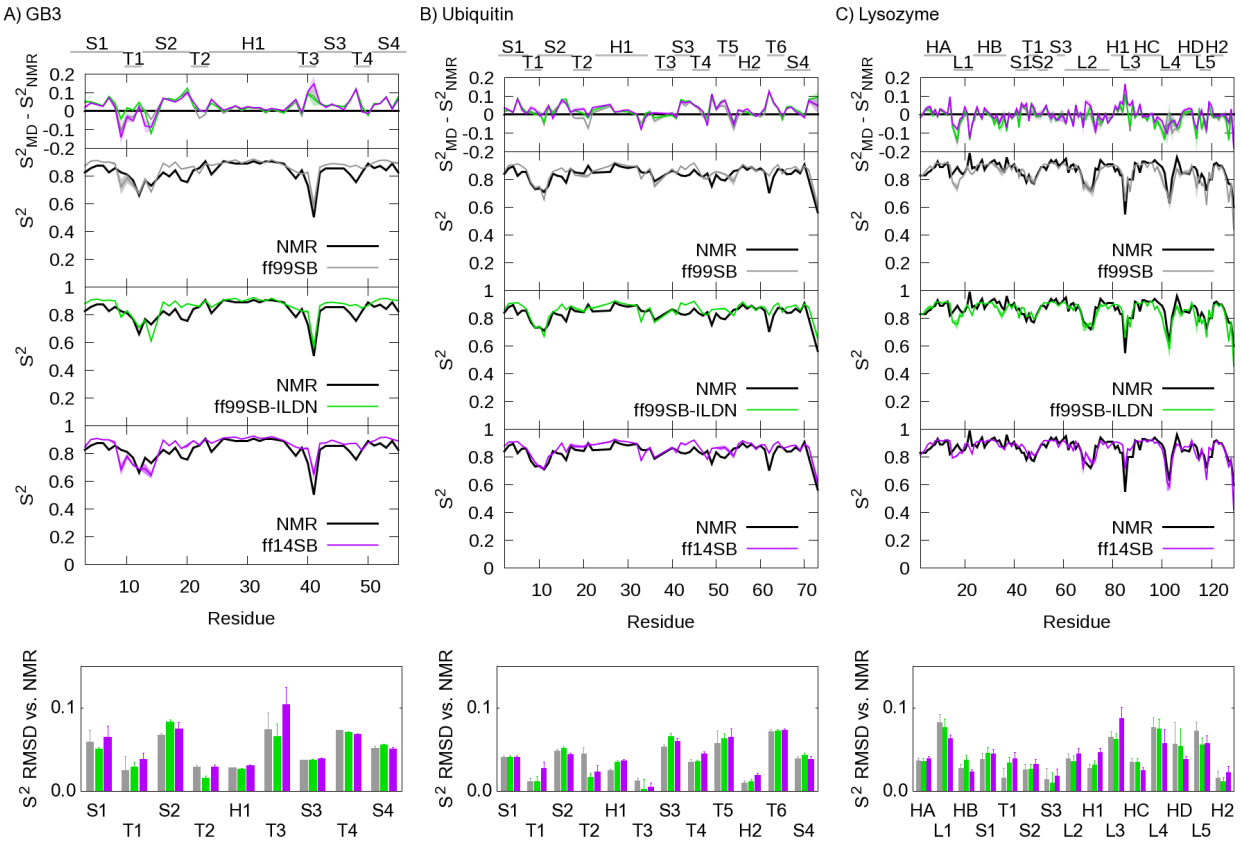

Figure S18: Order parameters from NMR compared to those back calculated by iRED for ff99SB, ff99SB-ILDN, and ff14SB simulations of GB3, ubiquitin, and lysozyme. Error bars represent the standard deviation of average values from four independent runs. The top panels show differences between simulation and experiment, while the lowest panels show average data for each secondary structure region, following Hornak et al. [10].

ff12SB

The ff12SB that was bundled with AMBER12[25] differs from ff14SB presented here in three ways. First, all four-atom dihedrals were frozen in the ff12SB training set structure minimization. This was done to reduce the influence of conformations with strong electrostatic interactions that resulted in different geometric distortions (e.g., in the amide planarity) between the QM and MM structures. This helped reduce the effect of strong electrostatics in residues like aspartate, but prevented covalent relaxation of steric clashes. By restraining only one 4-atom set per side chain rotatable bond in the ff14SB training set, but continuing to restrain all 4-atom sets in the backbone, the effect of electrostatic interactions was diminished while reducing the steric clashes in the training set, enabling a finer fit to quantum energies and subsequently better agreement with experimental scalar couplings.

A second problem arose when fitting corrections for different 4-atom sets describing rotation around the same bond, in which the periodicity of the corrections and the offsets between the 4-atom sets meant the corrections were in-phase (e.g., the N- and C- contributions to $\chi 1$ are separated by 120°, and thus the 3-fold corrections are in-phase). As corrections with such a relation have the ability to cancel, many of these corrections had large and potentially arbitrary magnitudes. In very small peptides like Val_3, $\chi 1$ corrections were observed to alter the relative positions of the main chain N and C, affecting backbone dynamics in ways that are difficult to predict. Therefore, corrections that are in-phase were forced to be identical to each other in ff14SB.

Third, ff12SB side chain corrections allowed phase shifts other than 0° or 180°. While this permitted slightly better agreement with quantum energies in some cases, it prohibits use of the same parameters as molecules change chirality, for example from L- to D-amino acids. Stereoisomers of a molecule should have the same energy, as they are *i*-symmetric with respect to each other. As all the dihedral angles negate in a stereoisomer, the phase shifts in dihedral corrections must also be negated. But a phase shift of 180° is equivalent to −180°, whereas 0° cannot be negated. Thus 0°/180° phase shifts avoid complications when

inverting chirality. Therefore, ff14SB corrections only employ 0°/180° phase shifts.

The difference in ff12SB and ff14SB training sets is significant for a few residues. In Figure S19, we show the errors of ff12SB and ff14SB against the sets of energies used to train each. Naturally, errors are lowest for each force field against its own training set. But ff12SB reproduces the energies of several residues in the ff14SB training set notably poorly. Whereas ff14SB is at most 1.2 ± 0.1 times the error of ff99SB (for threonine) against the ff12SB training set, ff12SB has 2.2 ± 0.4 times the error of ff99SB against ff14SB phenylalanine targets. After that, ff12SB has 1.8 ± 0.0 times the error for valine, 1.7 ± 0.1 times for tryptophan, and 1.4 ± 0.2 times for threonine. The ff12SB training generated parameters less appropriate for the ff14SB target energies of several residues than ff99SB.

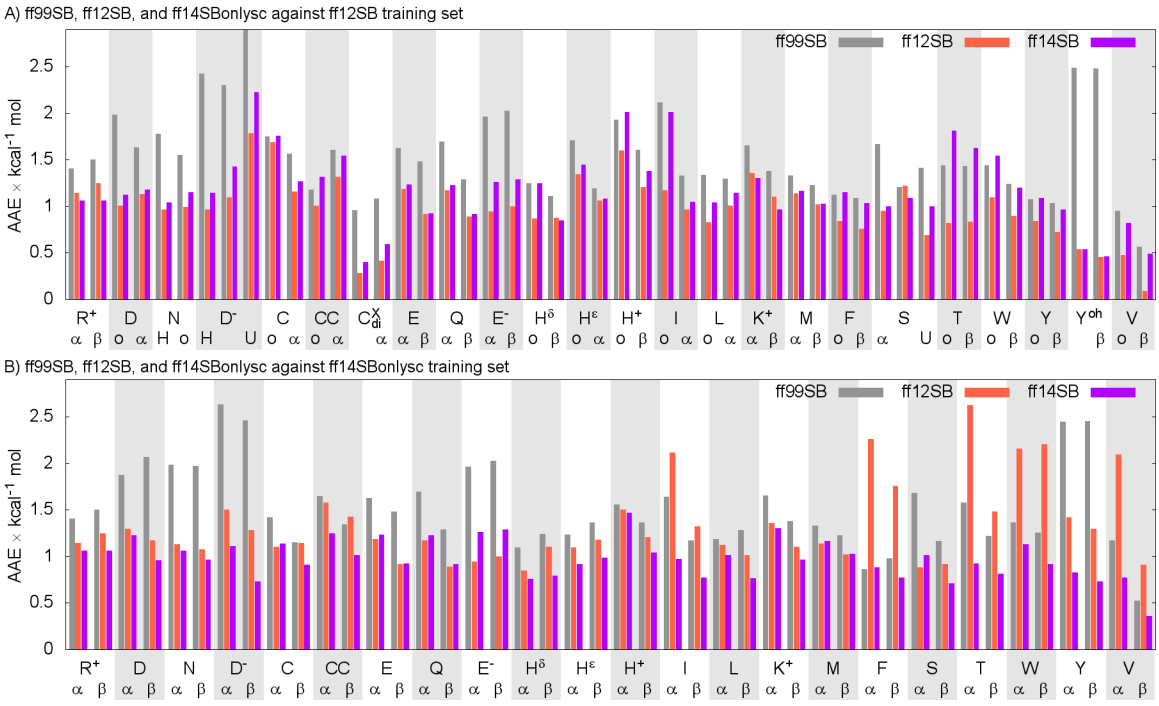

Figure S19: The errors of ff99SB (gray), ff12SB (tomato red), and ff14SB (purple) against the quantum mechanics energies used to train ff12SB (A) and ff14SB (B).

What's important is how such differences in the training affect accuracy of simulations in real systems. In Figure S20 on the following page, we illustrate some of these differences in GB3, ubiquitin, and lysozyme in terms of normalized error versus $\chi 1$ scalar couplings.[21,26–32] In fact, some residues improved dramatically, with aspartate and threonine normalized scalar

coupling errors being $39 \pm 7\,\%$ and $34 \pm 8\,\%$ better with ff14SB, respectively. Lysine, arginine, isoleucine, serine, valine, leucine, and tyrosine also improve by $29 \pm 7\,\%$, $22 \pm 15\,\%$, $20 \pm 11\,\%$, $19 \pm 8\,\%$, $16 \pm 12\,\%$, $14 \pm 12\,\%$, and $8 \pm 2\,\%$, although some of these differences approach insignificance. Phenylalanine and tryptophan are worse by $17 \pm 2\,\%$ and $5 \pm 2\,\%$, respectively, though the normalized errors in ff14SB are still quite small—0.08 ± 0.00 and 0.10 ± 0.00 for phenylalanine and tryptophan, respectively. Altogether, ff14SB better reproduces side chain scalar couplings by $17 \pm 3\,\%$ with a normalized error of 0.13 ± 0.00, compared with ff12SB's normalized error of 0.16 ± 0.00.

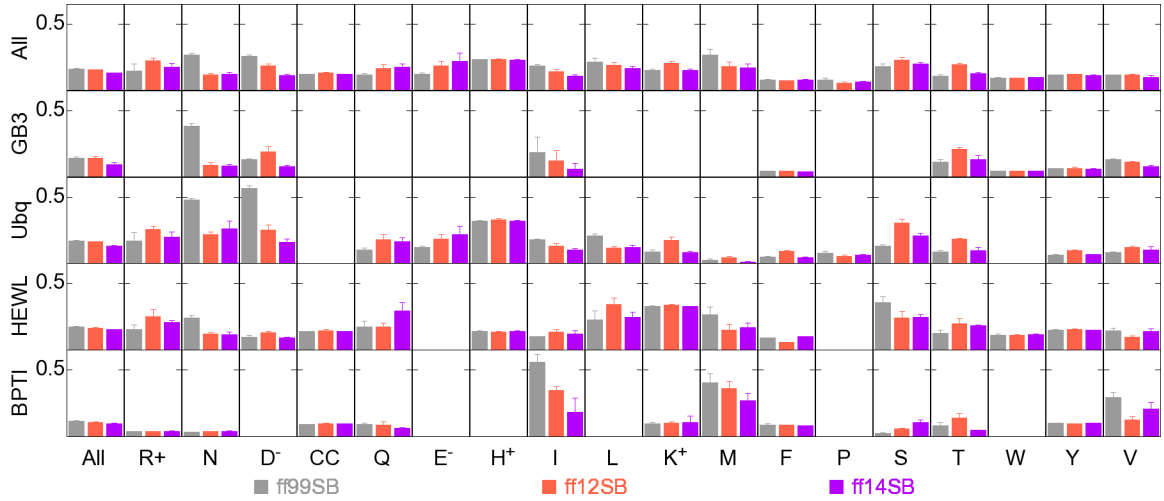

Figure S20: The mean absolute errors of simulations with ff99SB (gray), ff12SB (tomato red), and ff14SB (purple) compared to experimental J couplings, normalized by Karplus curve range, of all residues and each residue horizontally in all and each of GB3, ubiquitin (Ubq), and lysozyme (Lys) vertically. Error bars represent the standard error in the mean absolute errors of each independent run.

List of parameters

Table S8: ff14SB parameters

Correction	$n = 4$	$n = 3$	$n = 2$	$n = 1$
C -CX-2C-SH	0.075	0.251	-0.337	-0.269

Table S8: continued

Correction	$n = 4$	$n = 3$	$n = 2$	$n = 1$
N -CX-2C-SH	0.033	0.251	-0.486	0.154
N3-CX-2C-SH	0.033	0.251	-0.486	0.154
CX-2C-SH-HS	0.030	0.252	0.612	0.092
C -CX-2C-CO	0.154	0.058	-0.459	0.424
N -CX-2C-CO	0.089	0.058	-0.647	-2.154
N3-CX-2C-CO	0.089	0.058	-0.647	-2.154
CX-2C-CO-O2	-0.031		-0.769	
C -CX-2C-C	0.107	0.033	-0.303	1.046
N -CX-2C-C	0.059	0.033	-0.297	-0.688
N3-CX-2C-C	0.059	0.033	-0.297	-0.688
CX-2C-C -O				0.000
CX-2C-C -OH	-0.199	0.008	-0.575	-1.199
2C-C -OH-HO	0.113	0.479	-2.706	-0.448
CX-2C-C -N	0.008	-0.301	-0.485	-0.828
C -CX-CT-CC	0.025	0.219	-0.244	-0.143
N -CX-CT-CC	0.089	0.219	-0.221	-0.306
N3-CX-CT-CC	0.089	0.219	-0.221	-0.306
CX-CT-CC-NA	-0.037	0.686	-0.392	-0.16
CX-CT-CC-CV	-0.01	-0.122	0.750	-0.674
CX-CT-CC-NB	-0.047	0.740	0.204	0.690
C -CX-3C-CT	0.112	0.148	-0.289	-0.406
C -CX-3C-2C	0.115	0.113	-0.735	0.162
N -CX-3C-CT	-0.001	0.148	-0.216	0.337
N -CX-3C-2C	-0.097	0.113	-0.144	0.310

Table S8: continued

Correction	$n = 4$	$n = 3$	$n = 2$	$n = 1$
N3-CX-3C-CT	-0.001	0.148	-0.216	0.337
N3-CX-3C-2C	-0.097	0.113	-0.144	0.310
CX-3C-2C-CT	0.230	0.107	0.053	0.447
CT-3C-2C-CT	0.224	0.107	-0.077	0.202
C -CX-3C-OH	0.156	0.315	-0.119	-0.697
N -CX-3C-OH	0.095	0.315	0.006	0.674
N3-CX-3C-OH	0.095	0.315	0.006	0.674
CX-3C-OH-HO	0.013	0.236	0.251	-0.006
CT-3C-OH-HO	0.048	0.236	-0.079	0.643
C -CX-2C-3C	0.190	0.144	-0.62	0.706
N -CX-2C-3C	0.073	0.144	-0.259	0.098
N3-CX-2C-3C	0.073	0.144	-0.259	0.098
CX-2C-3C-CT	0.179	0.142	-0.027	0.379
C -CX-2C-OH	0.129	0.401	-0.218	-0.661
N -CX-2C-OH	0.160	0.401	-0.246	0.666
N3-CX-2C-OH	0.160	0.401	-0.246	0.666
CX-2C-OH-HO	0.007	0.267	0.444	0.211
C -CX-CT-C*	0.074	0.234	-0.353	-0.017
N -CX-CT-C*	0.031	0.234	-0.313	0.079
N3-CX-CT-C*	0.031	0.234	-0.313	0.079
CX-CT-C*-CB	-0.095	0.819	0.408	0.365
CX-CT-C*-CW	0.000	0.000	0.000	0.000
C -CX-CT-CA	-0.012	0.192	-0.469	0.055
N -CX-CT-CA	-0.007	0.192	-0.29	-0.012

Table S8: continued

Correction	$n = 4$	$n = 3$	$n = 2$	$n = 1$
N3-CX-CT-CA	-0.007	0.192	-0.29	-0.012
CX-CT-CA-CA	-0.048	0.000	-0.069	0.000
CA-C -OH-HO	0.065	0.000	-0.883	0.000
C -CX-2C-2C	0.145	0.144	-0.393	-0.421
N -CX-2C-2C	0.078	0.144	-0.184	-0.1
N3-CX-2C-2C	0.078	0.144	-0.184	-0.1
CX-2C-2C-C	0.138	-0.412	0.083	-0.196
2C-2C-C -O				0.000
2C-2C-C -OH	-0.066	-0.025	-1.104	-0.824
2C-2C-C -N	0.042	-0.085	-0.845	-0.609
CX-2C-2C-CO	-0.056	-0.608	-0.222	-1.367
2C-2C-CO-O2	0.064		-0.390	
CX-2C-2C-S	0.028	0.016	0.245	0.417
2C-2C-S -CT	0.057	0.414	0.442	-0.247
C -CX-2C-S	0.278	0.323	-0.394	0.602
N -CX-2C-S	0.064	0.323	-0.021	0.469
N3-CX-2C-S	0.064	0.323	-0.021	0.469
CX-2C-S -S	-0.135	0.302	0.666	0.056
2C-S -S -2C	0.379	0.682	4.480	0.420

References

(1) Bondi, A. *J. Phys. Chem.* **1964**, *68*, 441–451.

(2) Adams, D. *The Hitchhiker's Guide to the Galaxy*; The Hitchhiker's Guide to the Galaxy; Pan Books, 1979.

(3) Cornell, W. D.; Cieplak, P.; Bayly, C. I.; Gould, I. R.; Merz, K. M.; Ferguson, D. M.; Spellmeyer, D. C.; Fox, T.; Caldwell, J. W.; Kollman, P. A. *J. Am. Chem. Soc.* **1995**, *117*, 5179–5197.

(4) Bayly, C. I.; Cieplak, P.; Cornell, W.; Kollman, P. A. *J. Phys. Chem.* **1993**, *97*, 10269–10280.

(5) Frisch, M. J. et al. Gaussian 98. 1998.

(6) Wall, M. *Mechanical Engineering Department, Massachusetts Institute of Technology* **1996**,

(7) Lovell, S. C.; Word, J. M.; Richardson, J. S.; Richardson, D. C. *Proteins: Struct., Funct., Genet.* **2000**, *40*, 389–408.

(8) Graf, J.; Nguyen, P. H.; Stock, G.; Schwalbe, H. *J. Am. Chem. Soc.* **2007**, *129*, 1179–1189.

(9) Kosinska Eriksson, U.; Fischer, G.; Friemann, R.; Enkavi, G.; Tajkhorshid, E.; Neutze, R. *Science* **2013**, *340*, 1346–1349.

(10) Hornak, V.; Abel, R.; Okur, A.; Strockbine, B.; Roitberg, A.; Simmerling, C. *Proteins: Struct., Funct., Bioinf.* **2006**, *65*, 712–725.

(11) Song, K.; Stewart, J. M.; Fesinmeyer, R. M.; Andersen, N. H.; Simmerling, C. *Biopolymers* **2008**, *89*, 747–760.

(12) Honda, S.; Akiba, T.; Kato, Y. S.; Sawada, Y.; Sekijima, M.; Ishimura, M.; Ooishi, A.; Watanabe, H.; Odahara, T.; Harata, K. *J. Am. Chem. Soc.* **2008**, *130*, 15327–15331.

(13) Ulmer, T. S.; Ramirez, B. E.; Delaglio, F.; Bax, A. *J. Am. Chem. Soc.* **2003**, *125*, 9179–9191.

(14) Wlodawer, A.; Walter, J.; Huber, R.; Sjlin, L. *J. Mol. Biol.* **1984**, *180*, 301 – 329.

(15) Vijay-Kumar, S.; Bugg, C. E.; Cook, W. J. *J. Mol. Biol.* **1987**, *194*, 531–544.

(16) Young, A. C. M.; Dewan, J. C.; Nave, C.; Tilton, R. F. *J. Appl. Crystallogr.* **1993**, *26*, 309–319.

(17) Welch, B. L. *Biometrika* **1947**, *34*, 28–35.

(18) Travis, E. O. *Comput. Sci. Eng.* **2007**, *9*, 10–20.

(19) Jones, E.; Oliphant, T.; Peterson, P. SciPy: Open Source Scientific Tools for Python. 2001.

(20) Satterthwaite, F. E. *Biometrics* **1946**, *2*, 110–4.

(21) Lindorff-Larsen, K.; Piana, S.; Palmo, K.; Maragakis, P.; Klepeis, J. L.; Dror, R. O.; Shaw, D. E. *Proteins: Struct., Funct., Bioinf.* **2010**, *78*, 1950–1958.

(22) Prompers, J. J.; Brüschweiler, R. *J. Am. Chem. Soc.* **2002**, *124*, 4522–4534.

(23) Li, D.-W.; Brüschweiler, R. *J. Chem. Theory Comp.* **2011**, *7*, 1773–1782.

(24) Markwick, P. R. L.; Bouvignies, G.; Blackledge, M. *J. Am. Chem. Soc.* **2007**, *129*, 4724–4730.

(25) Case, D. A.; Cheatham, T. E.; Darden, H.; Gohlke, R.; Luo, R.; Merz, K. M.; Jr., A., Onufriev; Simmerling, C.; Wang, B.; Woods, R. *J. Comp. Chem.* **2005**, *26*, 1668–1688.

(26) Berndt, K. D.; Gntert, P.; Orbons, L. P.; Wthrich, K. *J. Mol. Biol.* **1992**, *227*, 757 – 775.

(27) Grimshaw, S. Novel approaches to characterizing native and denatured proteins by NMR.

(28) Hu, J.-S.; Bax, A. *J. Am. Chem. Soc.* **1997**, *119*, 6360–6368.

(29) Chou, J. J.; Case, D. A.; Bax, A. *J. Am. Chem. Soc.* **2003**, *125*, 8959–66.

(30) Miclet, E.; Boisbouvier, J.; Bax, A. *J. Biomol. NMR* **2005**, *31*, 201–216.

(31) Schwalbe, H.; Grimshaw, S. B.; Spencer, A.; Buck, M.; Boyd, J.; Dobson, C. M.; Redfield, C.; Smith, L. J. *Protein Sci.* **2001**, *10*, 677–688.

(32) Smith, L. J.; Sutcliffe, M. J.; Redfield, C.; Dobson, C. M. *Biochemistry* **1991**, *30*, 986–996.